HALMSTAD UNIVERSITY

Master's Programme in Electronic Design, 60 credits

MASTER THESIS

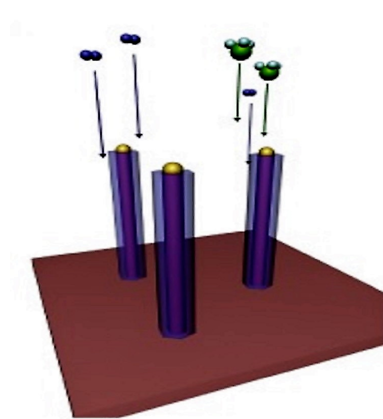

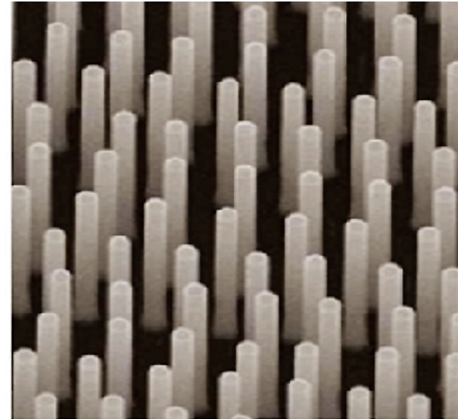

Studies on Radiation-induced Defects in InP/InAsP Nanowire-based Quantum Disc-in-wire Photodetectors

Ebrahim Mansouri

Nanoelectronics, 15 credits

Halmstad 2018-01-11

Studies on Radiation-induced Defects in InP/InAsP Nanowire-based Quantum Disc-in-wire Photodetectors

Master thesis in Electronic Design

2018

Author: Ebrahim Mansouri
Supervisors: Prof. Håkan Pettersson and Prof. Jan Pallon
Colleague: Dr. Linus Ros
Examiner: Dr. Pererik Andreasson

School of Information Technology
Halmstad University
PO Box 823, SE-301 18 HALMSTAD
Sweden

Studies on Radiation-induced Defects in InP/InAsP Nanowire-based Quantum Disc-in-wire Photodetectors

Ebrahim Mansouri

© Copyright Ebrahim Mansouri, 2018. All rights reserved.
Master thesis report ITE 12XX
School of Information Science, Computer and Electrical Engineering
Halmstad University
ISSN XXXXX

Preface

The need to understand radiation effects and to mitigate potential radiation damage in semiconductor devices and circuits has been growing in recent years. Space applications and military operations in radiation environments are obvious areas where intense high-energy radiation can lead to severe damage with serious consequences. Since many novel state-of-the-art electronic devices and sensors are based on advanced nanoscale structures, e.g. nanowires (NWs), it is important to investigate radiation-induced damage in such devices.

The aim of this project is to study degradation effects in InP/InAsP NW-based QDiscs-in-wire photodetectors exposed to high-energy particles to realize conceptually new types of sensitive imaging detectors. A mature technology for fabricating NW array photodetectors/solar cells has been developed at NanoLund group during last years. Moreover, it has recently been demonstrated that NWs are potential candidates for device applications in harsh radiation environments. The interaction of radiation with matter is a very broad and complex topic. Thus we have focused our work on explaining the most important aspects for understanding degradation effects in irradiated InP/InAsP NW-based array photodetectors.

This Master's thesis is a collaboration between NanoLund and the Department of Nuclear Physics, both at Lund University, and the School of Information Technology at Halmstad University.

Ebrahim Mansouri

Abstract

Photodetectors are used in many applications such as digital and thermal cameras or in solar panels. They can also be designed to detect the omnipresent high-energy radiation/particles, and for radiation imaging in biomedical applications. Novel nanostructures offer significant advantages compared to traditional designs for the realization of fast, sensitive, compact and cheap sensors and efficient solar cells. Examples of such nanostructures include quantum dots (QDs), quantum wells (QWs) and NW arrays.

This thesis is devoted to experimental investigations of effects of high-energy (1 MeV) protons on the optical and electrical performance of InP/InAsP NW-based QDiscs-in-wire photodetectors. The proton-induced degradation of the optical performance has been studied by means of Fourier Transform Infrared (FTIR) photocurrent spectroscopy. The spectrally resolved photocurrent (PC) and current-voltage (I-V) characteristics were measured at low temperature (5 K and 77K) and at room temperature (300K) before and after 1 MeV proton irradiation under vacuum conditions with fluences ranging from 1.0×10^{12}–3.0×10^{13} cm^{-2}. The particle radiation exposure has been done in the Ion Beam Accelerator at the Department of Nuclear Physics Department at Lund University.

Considering both PC and I-V characteristics, it was found that the devices were sensitive to all proton irradiation at all fluences. In general, the PC intensity significantly increased after radiation for all fluences, however, a week after exposure the PC and dark current gradually recovered. At 3×10^{12} p/cm^2 fluence level, it was figured out that photocurrent which attributed to QDiscs disappeared for a couple of days after exposure, however, over time and gradually, those started to manifest again even at low and room temperatures, causing radiation-induced changes in device parameters to be time-dependent; however, it was not recorded any signals related to QDiscs at fluence of 3×10^{13} p/cm^2. Substantial changes in the dark I-V characteristics, as well as increases in the dark current, are observed after irradiation. The influence of proton irradiation on light and dark current characteristics also indicated that NW structures are a good potential candidate for radiation harsh-environment applications. It was also observed a significant increase in dark current after the radiation for all devices, however, by applying the voltage to the photodetectors, the PC and I-V characteristics gradually being to diminish, which may be attributed to an annealing process.

Keywords: InP/InAsP, QDiscs-in-wire, photodetectors, proton irradiation, Photocurrent, I-V characteristics.

Contents

Preface ... i

Abstract ... iii

1 Introduction ... 1

2 Background ... 5

2.1 Introduction ... 5
2.2 Radiation environments ... 5
2.3 Fundamental radiation damage mechanisms on semiconductor devices ... 6
2.3.1 Ionisation damage ... 7
2.3.2 Displacement damage ... 9
2.4 Impact of radiation damage on semiconductor properties ... 14
2.4.1 Lifetime damage ... 14
2.4.2 Carrier removal ... 15
2.4.3 Mobility ... 16
2.5 Displacement damage in photodetectors ... 17

3 Sample specification and characterisation techniques ... 19

3.1 Photoconductors ... 19
3.2 Nanowire-based photodetectors ... 20
3.2.1 InP NW-based photodetectors ... 21
3.3 Growth, processing and sample specification ... 22
3.4 Characterization techniques ... 23
3.4.1 Fourier transform infrared spectroscopy ... 23
3.4.2 Fourier transform photocurrent measurements ... 25
3.4.3 Dark and photocurrent measurements ... 26

4 Experimental results ... 27

4.1 Pre-radiation FTPC and I-V measurements ... 27
4.2 Post-radiation FTPC and I-V measurements ... 30
4.2.1 Post-radiation PC measurements ... 30
4.2.2 Post-radiation I-V characteristics ... 33
4.3 Fluence-dependence of PC ... 34
4.4 Fluence-dependence of I-V characteristics ... 35

5 Conclusions ... 39

Acknowledgments ... 41

Bibliography ... 43

Chapter 1

1 Introduction

Study of radiation influences on optoelectronic components and electronic circuits is an essential segment of this field since it is impossible to imagine a world without various optical/electronic devices for ordinary life, scientific or military purposes. Moreover, for applications in satellite systems, energy spectrometry, gamma spectroscopy, *X*-rays dosimeters etc. devices based on novel nanomaterials offer significant advantages over traditional technologies in terms of radiation resist, light-weight and efficiency [1, 2]. However, the response of these devices to radiation effects is not well understood, and radiation effects modelling tools are not yet available. In the natural, high-radiation environment of space, all solar cells suffer from degradation. Although some studies have been conducted, and test data collected, on the performance of optoelectronic devices in a radiation environment, the mechanisms of radiation-induced degradation of NW-based photodetectors has yet to be established.

The negative influence of radiation on electronic devices was initially discovered during above-ground nuclear bomb tests in 1954 [3]. A False signal and malfunctions in the operation of the measuring equipment utilised during explosion tests were observed. Since 1960 further anomalies have been registered in electronic components and systems operating in space. Electronics of satellites were found to be unreliable at that time. Heavy-ions present in space generated soft errors in electronic systems and therefore disturbed the operation of transmitting modules of Explorer 1 in 1958 [4].

On the ground level single event upsets (SEUs)[1] were first reported during 2 kB dynamic random access memory (DRAM) tests. In that case, SEUs were not triggered by cosmic rays, but by alpha particles from the decay of Thorium and Uranium present in some integrated circuit packaging materials. It was the time when IBM first noticed a serious problem with memory reliabilities and initiated a research to understand the problem better. Later more cases of errors were observed in many applications including space, military and avionics. IBM employee James Ziegler noticed SEUs in commercial devices caused by cosmic rays at ground level [5].

Past and current research into III-V nanowires, such as InP, has opened up new avenues for device applications utilising their unique structural properties such as large surface area-to-volume ratio and carrier/photon confinement in 1D in devices such as single NW lasers [6], NW photodetectors [7, 8], and NW-based solar cells [9, 10]. Optoelectronic devices have a wide range of space applications, such as

[1] **SEU** is a change of state caused by one single ionising particle (ions, electrons, photons...) striking a sensitive node in a micro-electronic device, such as in a microprocessor semiconductor memory etc.

photodetectors for optical communications [11], photo sensors for imaging [12], and solar cells for energy harvesting [13]. In space, it is required that all devices preserve their functionality in a hostile space environment throughout the life of the mission. An important feature of this environment is the existence of radiation of various types such as high-energy electrons, protons, neutrons, gamma-rays or *X*-rays [14]. Based on statistics, in the geostationary orbit for 10–15 years application, the total fluence of proton particle energy > 1MeV imparted on the devices should be less than 1×10^{13} cm^{-2} [15].

In contrast to purely hit-and-miss material development for specific applications, the atomic-scale design aims to achieve superior radiation response by purposefully manipulating the composition and nanostructure to control the behaviour of radiation-induced defects, which typically depends on modelling to determine the impact of these modifications on material properties [16].

In accordance with the energy, the effects of high-energy particle/photon radiation on optoelectronic devices can be divided into two main categories: (a) the excitation of electrons, (b) disturbance of the periodic structure of the crystal, i.e., the formation of "structural radiation defects". Studies in heterojunction bipolar transistors (HBTs) based on InP/InGaAs have shown that the reliability of these devices in radiation environment is an important issue particularly in space-based communication systems [17]. The electron [18], neutron [19], and proton [20] irradiation performance of InP/InGaAs HBTs has been investigated extensively in recent years. In addition, investigations on GaAs metal-semiconductor field-effect transistors (FETs) show that the source and drain regions are more sensitive to the single event effect, and the ionising effect typically occurs at the semiconductor-insulator interface. Therefore, for solar cells and photodetectors used in space and other radiation environments, the most concern arises from the displacement damage effect, which primarily reduces the minority carrier lifetime, mobility and carrier concentration [2]. Device performance that depends on these parameters will be affected by displacement damage. In recent decades, a considerable number of papers have been published on the radiation effects in both conventional [21, 22] and quantum well [23, 24] structures.

The continued interest in InP-based technologies, as a prospective candidate for the fabrication of particle and radiation detectors, has been shown in works published over the last few decades. The relatively large effective atomic number of In (49), which provides high *X*- and γ-ray stopping power above 10 keV, as well as the high electron mobility and large bandgap (1.34 eV) make InP an attractive material for application as fast-response detectors promising a high charge collection efficiency (CCE) at room temperature. To date, there have been several tests to determine the total dose performance of InP-based transistors [25, 26]. These tests have consistently found that InP devices show little degradation even at large total dose levels. In one case [27], the

collector current was seen to degrade by only 9% at a total dose equivalent to 620 Mrad(Si)[2].

This thesis is a report on the amount of endurance and tolerance of InP/InAsP photodetectors based on NW technology used in radiation-harsh environments. Considering the previous studies on the growth, fabrication and characteristics of this new type of detector, we intend to investigate on the potential applications as a particle detector along with scintillator material by completing information on the tolerance of this material in high energy environments. The scope of this work is to understand the degradation mechanism of proton radiation on NW-based photodetectors and who these induced-defects change the optoelectronic properties of our devices, and finally to give a perspective on their potential as optoelectronic components, specifically as high-energy particle detectors. Moreover, it is supposed to examine and devaluate the radiation tolerance of this Nano-scale photodetectors with the scope of being used in radiation-harsh environments at the next stage.

The thesis is divided into five chapters. The description of their contents is presented below:

- Chapter 1: A short introduction describing a historical background and previous studies on radiation tolerance of optoelectronic devices in radiation-harsh environments is presented, and finally it ends with the aim of ongoing research.
- Chapter 2: Radiation environments and effects of energetic particles radiation, e.g. proton, on various electronic components and circuits are theoretically discussed in Chapter 2. The ionising and displacement damage are crucial to understand the impacts of radiation and how those effects in turn change the carrier lifetime, carrier removal and mobility.
- Chapter 3: To clarify the exposed devices, sample specifications and characterisation techniques are gathered.
- Chapter 4: All experimental results before and after radiation are collected. Moreover, the results are compared pre- and post-radiation. Besides, a technique used for the design of radiation-hardened devices are summarised in this chapter.
- Chapter 5: Finally, the conclusion an outlook of this work is presented in the last chapter.

[2] Rad: Radiation absorbed dose. Original measuring unit for expressing the absorption of all types of ionising radiation (proton, beta, gamma, etc.) into any medium. The SI unit for absorbed dose is the gray, defined as 1 j/kg (1 Gy = 100 rads), but the rad is more commonly used.

Chapter 2

2 Background

2.1 Introduction

This chapter provides an overview of radiation environments and basic radiation damage mechanisms in semiconductor devices. Subsequently, the different impact of photon/particle irradiation on the device performance will be briefly discussed, which can be defined as the macroscopic damage or degradation.

Generally speaking, radiation has always been present in the natural environment and sources of energetic radiation are commonly found in water, air, soil, or manmade devices. Particle radiation is the radiation of energy by means of fast-moving subatomic particles. Particle radiation is referred to as a particle beam if the particles are all moving in the same direction, similar to a light beam. Due to the wave–particle duality, all moving particles also have wave character. Higher energy particles more easily exhibit particle characteristics, while lower ones more easily exhibit wave characteristics. Charged particles (electrons, mesons, protons, alpha particles, etc.) can be produced by particle accelerators as well. For instance, ion irradiation is widely used in the semiconductor industry to introduce dopants into materials, a method known as ion implantation. Radiation can have harmful effects on solid materials as it can degrade their properties so that they are no longer electronically stable.

2.2 Radiation environments

The amount of radiation that semiconductor devices and materials encounter during their lifecycle strongly depends on the radiation environment and their operating conditions. For space missions and military applications, it is obvious that there is a radiation-harsh environment. However, also during their fabrication process and even for standard terrestrial operation, the devices may suffer from ionising radiation.

In general, one can differentiate between the following different environments:

- Space
- High-energy physics experiments
- Natural environments
- Nuclear reactors
- Processing-induced radiation

Each of these environments is characterized by its own spectrum of particles and energy distribution. For instance, the main sources of energetic particles in a space

environments are protons and electrons trapped in the Van Allen belts, heavy ions trapped in the magnetosphere, cosmic ray protons and heavy ions, and protons and heavy ions from solar flares. The radiation level of these sources strongly depends on the activity of the sun. The Van Allen belts, consist mainly of electrons up to a few MeV in energy and protons of up to several hundred MeV trapped in the earth's magnetic field.

Moreover, the fabrication of modem semiconductor devices relies on several numbers of processing steps which can induce radiation-damage [28]. Typical examples are ion implantation, dry etching, e-beam or *X*-ray lithography, plasma enhanced chemical vapour deposition, etc. Although the degree of introduced damage is much lower than for the other radiation environments mentioned above, state-of-the-art devices are very vulnerable to. Detailed discussions on radiation environments can be found in [29, 30].

2.3 Fundamental radiation damage mechanisms on semiconductor devices

The study of radiation effects in semiconductor electronics and the development of radiation-resistant integrated circuits have formed an active scientific community that has produced a wealth of data and conceptual understanding. Although access to some of these results and techniques is restricted, most of the data and papers are in the public domain and readily accessible, and they provide a valuable source for investigation.

This is a very complicated field and developing a general road map is not easy, but one can apply a few fundamental considerations to understanding the effects of radiation on device types in specific circuit topologies and narrow the range of options that must be studied in detail. In general, semiconductor devices are affected by two basic radiation damage mechanisms. A distinction can be made between ionisation damage, on the one hand, which creates free electron-hole pairs by disrupting electronic bonds and displacement damage, on the other, giving rise to atoms which are displaced from their usual lattice site, leaving behind a vacancy. The former mechanism requires generally far lower energies than is necessary for displacement damage. A further differentiation can be considered between prompt or fast effects, like Single Event Upsets (SEU) or Latch-up (SEL) and more permanent (hard) damage. A more detailed description of the damage mechanisms can be found in text books [29, 30].

Both mechanisms are important in detectors, transistors and integrated circuits. Some devices are more sensitive to ionisation effects; some are dominated by displacement damage. Hardly a system is immune to either one phenomena and most are sensitive to both.

2.3.1 Ionisation damage

Ionisation damage is a dominant mechanism when energetic photons (X and γ-rays) interact with solid-state matter. Based on the photon energy E_{ph}, different fundamental interactions can take place, as shown in Fig. 2.1 [31], which result in the creation of an energetic free carrier (or pair) in the material. At the lower end of the spectrum (soft X-rays of a few keV) complete absorption of the photon energy by the emitted electron occurs, which is the well-known photoelectric effect. It should be pointed out that according to the incident photon energy, two kinds of photoelectric effects can be distinguished. In case of a semiconductor, the emission of electrons from valence band to conduction band (band-to-band excitation) when the photon hits the material is called internal photoelectric effects. In that case, the electron does not leave the material, but also jumps into the conduction band, leaving behind a free hole and move freely throughout the material. The net result is the creation of a free electron-hole pair. However, in external photoelectric effects, because of much more transferred energy by incident photon to the electron in valence band, it can easily release the electron from material.

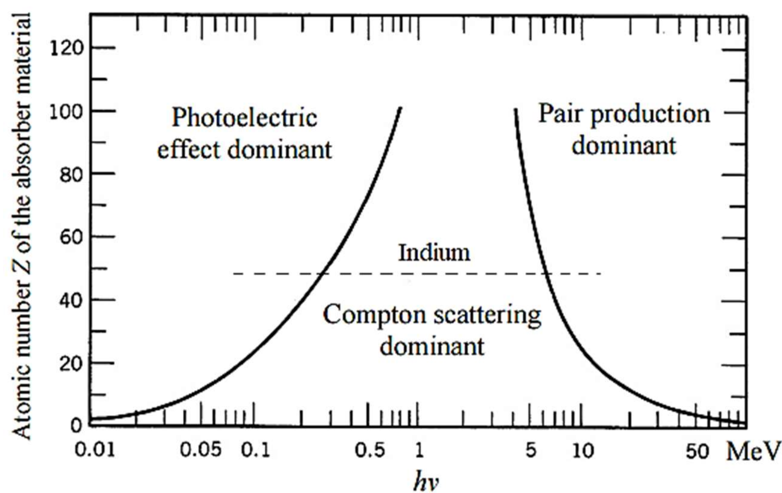

Figure 2.1: Illustration of the relative importance of the three photon interactions with target materials. The solid lines correspond to equal interaction cross sections for neighbouring effects. The dashed line represents the situation for Indium (Z=49).

For intermediate photon energies the Compton effect dominates, whereby an incomplete absorption of the photon energy occurs, i.e., a secondary lower energy photon is emitted in addition. If the energy is above the threshold, this photon can again be absorbed to generate a second electron-hole pair, etc. As a result, an average number of $E_{ph}/E_{e\text{-}h}$[1] carrier pairs will be generated in the semiconductor material, which

[1] $E_{e\text{-}h}$: electron-hole pair ionisation threshold energy(eV).

is proportional to the original photon energy. This forms the basis of nuclear-radiation spectroscopy using semiconductor detector diodes.

Finally, for energies above the threshold of 1.02 MeV, electron-positron pair production will become important. The limits of equal probability are represented in Fig. 2.1. The probability for the different processes is generally described by the interaction cross section, which can show strong discontinuities (e.g., thresholds) as a function of the photon/particle energy. It should be noted that electron-hole pair formation is also an important energy loss mechanism for high-energy electron and ion irradiation, while it is of secondary importance for neutron exposures.

The amount of energy deposited in the material through ionising interactions is determined by the stopping power (or Linear Energy Transfer function) $\rho_m^{-1}\, dE/dx$ (in MeV cm^2/g) where ρ_m is the density of the material and E the radiation energy; dx is an elementary trajectory in the material. The stopping power depends on the target material, the type of particle and its energy. That can be theoretically expressed by the following formula [29]:

Equation 2-1
$$-\frac{dE}{dx} = 2Pe^4 Z_1^2 Z_2 N_{at} \frac{M_2}{m} \frac{1}{E} \ln\left(\frac{4E}{E_{e-h}}\right)$$

where Z_1 and Z_2 are the atomic charges of the incident particle and the target material, N_{at} is the atomic density of the target, M_2 the corresponding atomic mass, m and E are the mass and energy of the incident particles and E_{e-h} is the mean ionisation energy, defined above. Furthermore, e is the electron charge in absolute value and P the stopping number of the material, which rises slowly with the energy.

For charged particles, the most likely interaction is with electrons in the target material because electrons occupy most of the atomic volume. In this process, referred to as ionisation loss, a small amount of energy, typically a few eV, is transferred to an electron by the incoming particle. For a semiconductor or insulator, this energy is absorbed by an electron in the valence band, raising it to the conduction band, and creating a corresponding hole in the valence band. Thus, ionisation creates an electron-hole pair in the material. This is shown pictorially in the E-k diagram of Fig. 2.2.

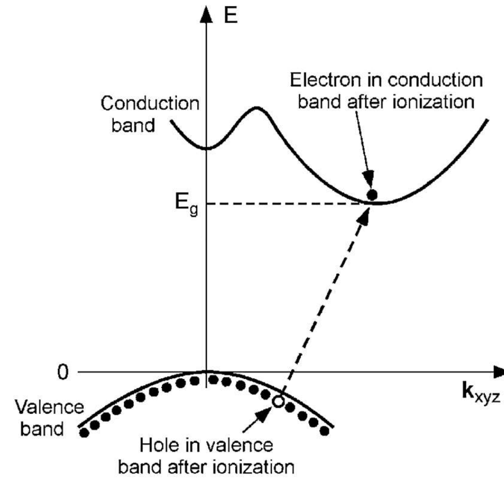

Figure 2.2: Creation of an electron-hole pair by ionisation in a semiconductor or insulator.

When ionisation is produced by photons, the minimum energy required to create an electron-hole pair is the bandgap energy, E_g, because the photon is directly absorbed by the valence band electron. However, the process is more complicated for high energy particles. Ionisation from a heavy particle is the result of a shower of secondary electrons, which have a mean free path that overlaps several lattice positions.

Part of the deposited energy is dissipated through other processes, including weak interactions with other electrons that do not result in ionisation. For this reason, the minimum amount of absorbed energy required to create an electron-hole pair from high-energy particles is larger than for photon absorption. The minimum energy depends on the particle type and energy. It is typically between 2.2 and 4 times the bandgap energy [32]. Table 2.1 shows the bandgap and minimum energy for electron-hole creation through ionisation for several semiconductors.

Table 2.1: Bandgap and energy for electron-hole pair production by ionisation for several semiconductors [33].

Material	E_g (eV)	Minimum energy to Produce an Electron-hole pair (eV)
Si	1.12	3.6
InP	1.35	4.5
GaAs	1.43	4.7
4H-SiC	2.86	8.5

2.3.2 Displacement damage

The second mechanism is displacement damage, which moves lattice atoms away from their normal position, disrupting the regular atomic spacing within the material. Before discussing displacement damage, it is instructive to briefly review some

important results for particle scattering. Particle collisions can be divided into two general categories: elastic scattering, where the total energy of the incident particle and target is unchanged by the scattering event; and inelastic scattering, where additional energy is lost or gained during the collision through other processes, such as nuclear reactions. Many interactions of space radiation can be understood from the standpoint of Rutherford scattering, which describes scattering of two charged particles. The primary particle has charge Z_1e and momentum m_1v_0. That particle interacts through electrostatic forces (Coulomb scattering), with a target particle of mass m_2 and charge Z_2e. The extrapolated direction of the initial path of the incoming particle (without considering the change in angle from scattering) comes within a distance b (is called the impact parameter) of the initial site of the target particle, as shown in Fig. 2.3. For the range of energies encountered by protons in space, nonrelativistic scattering can be used, but relativistic scattering must be used for electrons.

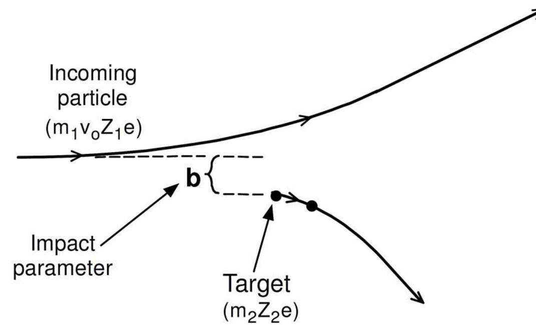

Figure 2.3: Diagram of the Rutherford scattering process [33].

The distribution of scattering angles of the incoming particle is inversely proportional to the fourth power of the sine of ½ the scattering angle. Consequently, only a small fraction of the particles is scattered at large angles (an angle of 180° corresponds to backscattering), provided that the mass of the incoming particle is less than that of the target particle. That condition corresponds to maximum energy transfer from the incoming particle to the target particle. For the nonrelativistic case, the maximum energy that can be transferred in an elastic collision is

Equation 2-2
$$E_{max} = 4E_{inc}\left[\frac{m_1 m_2}{(m_1 + m_2)^2}\right]$$

where E_{max} is the maximum transferred energy, E_{inc} is the energy of the incoming particle, m_1 is the incident particle mass, and m_2 is the target atom mass.

Displacement damage occurs where an incident particle transfers enough energy to knock out the target atom from its normal lattice position to another position, creating behind a vacancy (V) and an interstitial (I) position in the lattice. Such one-atom disorder in a crystalline lattice is called a point defect. The interaction can either be electromagnetic (for charged particles with lower energies) or through nuclear

interactions. These primary radiation defects are highly mobile at room temperature and will, therefore, migrate a long distance. They can either disappear from the material, by recombination at the substrate or other sinks or become trapped by impurity atoms giving rise to more stable secondary defects or to defect complexes. The probability for such atomic displacements is higher for higher E and m.

The threshold energy, which is the minimum energy that must be absorbed by a lattice atom to move it from its normal position, is closely related to crystal binding energy and is roughly correlated with the reciprocal of the lattice spacing. The threshold energy is approximately 8 eV for InP and about 10 eV for GaAs [33]. Table 2.2 shows the displacement threshold energy for several semiconductors. In general, semiconductors with high threshold energy will be more resistant to displacement damage because of the higher threshold energy.

Table 2.2: Displacement threshold energy for several semiconductors [33].

Material	Displacement energy threshold (eV)
InAs	7.4
InP	7.8
GaAs	9.5
Si	12.9
Ge	14.5
GaN	19.5
4H-SiC	21.3

A wide range of energies can be transferred to the lattice atom by the mechanisms that produce displacements. The part of the energy that goes into lattice damage is often called Non Ionising Energy Loss (NIEL) [34]. For the case where a relatively small amount of energy is absorbed, that is, energies of the same order as the threshold energy, a vacancy-interstitial pair (Frenkel pair) is formed where the vacancy and interstitial atom are located close together. This is illustrated in Fig. 2.4.

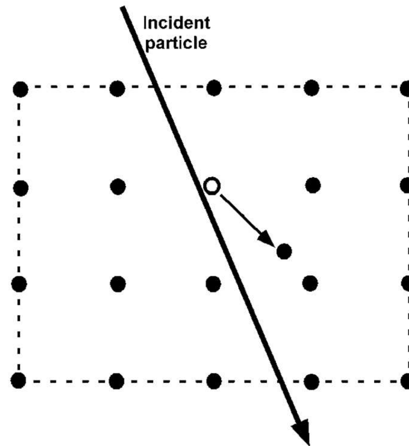

Figure 2.4: Diagram of displacement of a lattice atom forming a vacancy-interstitial pair [33].

The microscopic nature of the damage is quite different for more energetic collisions, where the energy absorbed by the lattice atom is much higher than the threshold energy. The atom involved in the primary interaction with the incident radiation particle is called the *primary knock-on atom* (PKA). If the PKA energy is much greater than the displacement energy threshold, it will have sufficient energy to interact with several other atoms in the lattice before it stops, creating additional atomic displacements.

2.3.2.1 Displacement damage from protons and heavy ions

Interactions of high energy particles depend on the mass and energy of the incoming particle as well as the mass of the target atom. Displacement damage for more massive charged particles can be produced when their velocity is well below the speed of light. For an incident charged particle with low energy (compared to its rest mass), the transit time is long enough so that the more tightly bound electrons in the target atom can move in response to the electric field from the particle strike, increasing the effective size of the nucleus in the collision process.

The PKA's atoms or recoil atoms displaced by a high-energy particle can vary in kinetic energy from near zero up to some maximum determined by collision kinematics. These PKAs in turn can produce additional vacancy-interstitial displacements by further collisions and if they are generated with sufficient energy additional damage cascades will be formed. The resulting damage along an individual particle path becomes quite complex and may be composed of the initial cascade and branching terminal sub-clusters, represented in Fig. 2.5 [35]. This is also often termed cluster damage.

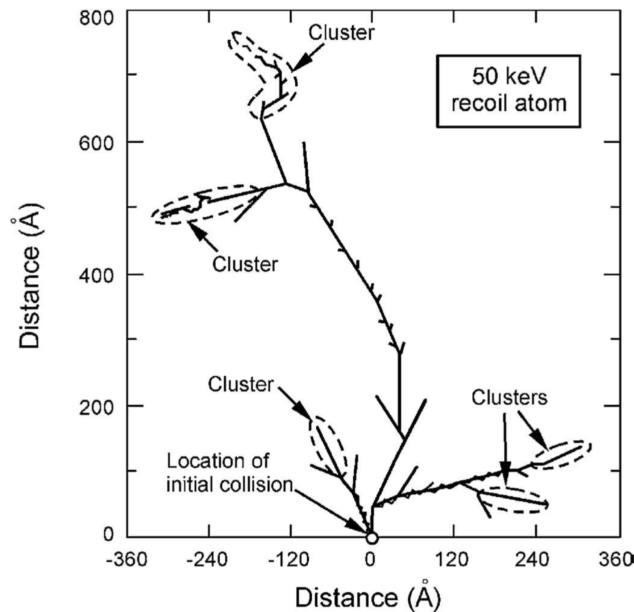

Figure 2.5: Monte Carlo simulations of displacement damage in silicon for the case that the energy transferred to the lattice site is more than 1000 times greater than the threshold energy for displacement [35].

Figure 2.5 shows the results of a Monte Carlo calculation of displacement damage in silicon for the case where 50 k*eV* of energy, about 4000 times greater than the displacement threshold energy, is transferred to the PKA [35] using a more sophisticated model that accounts for cluster defects. In this example, the atom follows a tortuous path through the lattice, creating two basic types of damage: vacancy-interstitial pairs, and large *cascade damage* regions, as shown in the figure. The displaced lattice atom finally stops about 70 *nm* away from its original position, a distance corresponding to several hundred lattice sites from its original position. Although this calculation is for silicon, the same process occurs in other materials. The important point is that the microscopic nature of the damaged region is very different for the case where high amounts of energy are absorbed by the lattice atom. The cascade damage regions extend over many lattice sites and are charged after they are formed, as well as disrupting the crystal lattice over an extended region. They are usually unstable, except at low temperature. Part of the damage may recover after irradiation (annealing). Annealing in GaAs, as well as for most other materials, depends on charge injection after the damage has occurred [33]. Thus, passing current through an irradiated device will accelerate the annealing process.

The difference in microscopic damage for various particles and energies is extremely important. Incident particles with low energy produce Frenkel pairs. Particles with higher energy also produce Frenkel pairs, but also create cascade regions where there are many displaced atoms in a localized region. The approximate amount of energy that must be transferred to a lattice atom to produce cascade damage regions is 1000 *eV* [33].

The complex lattice structure of compound semiconductors makes it more difficult to analyse displacement processes compared to a material with only one type of atom. For a binary compound such as InP, the threshold energy is different for the two atomic species because they have different crystal binding energies. The range of the displaced atom and its effect on the lattice also depends on the collision angle. However, those distinctions are usually unimportant when we consider the effects of many such collisions on macroscopic device properties unless we are dealing with low energy particles that have barely enough energy to displace individual atoms.

2.4 Impact of radiation damage on semiconductor properties

In the foregoing, two types of basic radiation-damage mechanisms have been described. As will be seen next, they also have a different impact on the device performance, which can be defined as the macroscopic damage or degradation. Besides the damage mechanism, one should also consider the time scale on which the effects play, as the primary damage (i.e. electron-hole or V-I pairs) undergo different kinds of interaction after their creation. In many cases, the degradation of a certain device parameter, for example the reverse current I_R of a diode, can be described by a so-called damage factor or parameter K_{IR}. It is defined as the change of the parameter with total dose (ionisation) or particle fluence (displacement). As will be shown, often there exists a good correlation between these factors and the energy deposited by ionising or non-ionising energy loss. In other words, they are useful in the modelling or even prediction of the device/circuit degradation in a radiation environment without the need to know the exact details of the microscopic defects formed during the exposure. In the next part, it will be briefly outlined how these damage factors can be used for that purpose.

2.4.1 Lifetime damage

Early radiation effects studies noted that the semiconductor parameter most affected by displacement damage was minority carrier lifetime, which becomes shorter after damage occurs. Studies of basic materials showed that the minority carrier lifetime could be related to particle fluence by the equation 2-3 [36]:

Equation 2-3
$$\frac{1}{\tau} - \frac{1}{\tau_o} = \frac{\Phi}{K_{tau}}$$

where τ is the minority carrier lifetime after irradiation, τ_o is the initial minority carrier lifetime, Φ is the particle fluence (particle/cm^2), and K_{tau} is the lifetime damage constant (cm^{-2}-s per particle). The damage constant, K_{tau}, depends on particle type, particle energy, (and for some semiconductors the injection level), and is really only constant under a restricted set of conditions.

Lifetime degradation can often be related to electronic device properties. One example is bipolar transistor technologies for the case where the gain is limited by recombination in the base region. Lifetime damage also affects solar cells and photodetectors which often depend on charge collection by diffusion. Lifetime damage is of secondary importance for junction field-effect transistors (JFETs) and metal-semiconductor field-effect transistors (MESFETs) because they are majority carrier devices.

Relatively few lifetime damage studies have been done at the device level for compound semiconductors. Table 2.3 compares lifetime damage constants for 50-MeV protons in a silicon transistor with damage constants for compound semiconductor LEDs [33]. Note the much higher values for the two wide-bandgap semiconductors, which causes them to be much less sensitive to radiation damage.

Table 2.3: Lifetime Damage Constants for 50-MeV Protons in Various Materials [33].

Device Structure	Material	Approximate Doping level (#/cm^3)	Damage Constant [cm^2-s/p]
Silicon Transistor	P-silicon (base region)	5 x 10^{17}	~ 7 x 10^5
GaAs LED	N-GaAs (Si doped)	~ 10^{19} (compensated)	~ 3 x 10^4
GaN LED	Undoped	Unspecified	~ 10^7
6H-SiC	Unspecified	Unspecified	~ 4 x 10^7

2.4.2 Carrier removal

A second mechanism, which is most often the dominant damage mechanism for compound semiconductors, is carrier removal. This process occurs because radiation-induced defects within the bandgap can trap some of the majority carriers from dopant atoms that are normally ionised to produce carriers within the valence or conduction band. This effectively changes the doping density as the number of defects increases during irradiation. The basic relation (shown here for an n-type semiconductor) is

Equation 2-4
$$n - n_o = R_c \Phi$$

where n is the minority carrier density, n_o is the initial minority carrier density before irradiation, R_c is the carrier removal coefficient in cm^{-3} per particle/cm^2, and Φ is the particle fluence [33]. If the number of defects is small, the Fermi level will remain unchanged. However, as the number of defects increases, they will affect the bandgap, depending on the position of the recombination centres in the bandgap relative to the energy of the dopant atoms. Defect centres that are located deep at or near the mid-

bandgap are generally more effective in the carrier removal process compared to shallow defects, and the carriers that are captured are more thermally stable compared to shallow defects.

As the bandgap changes, the linear relationship implied by Equation 2-4 will no longer apply, causing the carrier removal coefficient to change with fluence. R_c is usually constant as long as the change in carrier density is <25% [33], but for compound semiconductors we are often concerned with fluences that are high enough to produce larger carrier densities. However, other compound semiconductors have not been studied as extensively as GaAs. Messenger, et al., determined that carrier removal in InP was independent of carrier concentration over the range of 10^{16} to 4×10^{17} cm^{-3}, using solar cell data [37]. It is outside the scope of this work to give a detailed discussion of the vast amount of literature on carrier removal. For a thorough discussion, the interested reader is referred to [29, 38].

2.4.3 Mobility

Mobility is also affected by displacement damage because of impurities within the bandgap increase carrier scattering. Mobility changes can be described by

Equation 2-5
$$\frac{\mu_o}{\mu} = 1 + \beta\Phi$$

where β is the damage constant that applies to this process. Damage constants for mobility are lower than for lifetime damage or carrier removal, and consequently the effect of displacement damage on mobility is usually only important at very high fluences. McGarrity, et al., developed a relationship between carrier removal and the mobility damage constant that is applicable when the damage is low enough to prevent the Fermi level from changing [39]. They assumed that the carrier removal rate is equal to the introduction rate of recombination centres, then the mobility can be expressed as

Equation 2-6
$$\mu = \mu_o \left(1 + \chi \frac{\Delta n_o}{n_o}\right)^{-1}$$

where μ is the mobility after irradiation, μ_o is the initial mobility, Δn_o is the change in carrier concentration, n_o is the initial carrier concentration, and the parameter χ is defined as

Equation 2-7
$$\chi = \frac{\mu_o}{\alpha}$$

with α the coefficient that describes the (linear) relationship between the change in mobility and the change in mobility due to Coulomb scattering from charge centres.

Fig 2.6 indicates how minority carrier lifetime, carrier density, and mobility of a GaAs LED depend on proton fluence (all three are normalized to their pre-irradiation values) [33]. Initial values were as follows: lifetime, 0.9 μs; carrier concentration 3 x 10^{16} cm^{-3}; and mobility, 6500 $cm^2/(V\text{-}s)$. The lifetime results are direct measurements, while the values for carrier concentration and mobility are calculated. Note the extreme sensitivity of minority carrier lifetime to radiation damage compared to the other parameters. If the initial lifetime value was an order of magnitude lower (0.09 μs), the fluence dependence for lifetime damage would shift by one order of magnitude to right, while the fluences for changes in carrier concentration and mobility would be about the same.

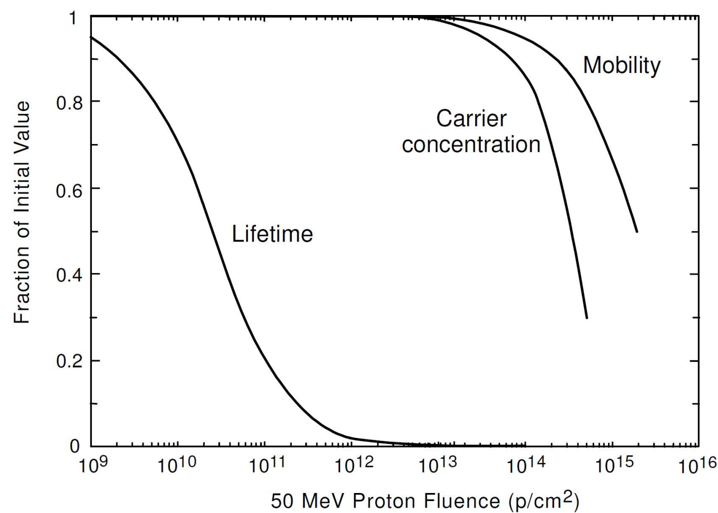

Figure 2.6: Degradation of minority carrier lifetime, carrier concentration, and mobility for a GaAs light-emitting diode after irradiation with 50 MeV protons

This suggests why the few types of compound semiconductors that require long lifetimes for their electrical performance are highly sensitive to displacement damage, while the majority of compound semiconductor devices are relatively resistant to displacement damage effects. Note that the fluence range in Fig. 2.6 between lifetime damage and changes in carrier concentration (or mobility) is about five orders of magnitude!

2.5 Displacement damage in photodetectors

Displacement damage in optoelectronic devices varies over an extremely wide range. Some types of devices are among the most sensitive to displacement damage effects, degrading significantly even in low-radiation environments. Others are extremely

tolerant to radiation damage. This wide range in radiation damage sensitivity is related to device design and basic operating principles [40, 41, 42].

A comparison of proton damage in an InGaAs detector with a conventional silicon p-n detector is presented in Fig. 2.7. The InGaAs detector degrades at a radiation level that is about two orders of magnitude higher than the silicon detector. Similar results were reported by Marshall and Dale [43].

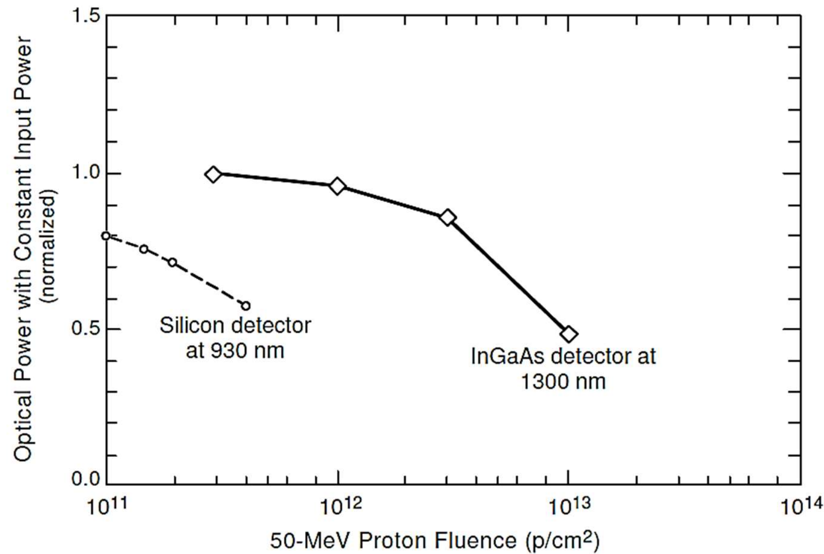

Figure 2.7: Comparison of proton damage in an InGaAs detector, measured at 1300 nm, with damage in a conventional silicon detector, measured at 930 nm [33].

Unpublished results show that the spectral width of the 1300 nm detectors is affected by radiation damage, but that the responsivity at the peak wavelength is less affected than regions away from the peak. Results for detectors optimized at 1300 nm are not necessarily applicable to other InGaAs detectors, and more research is needed to fully understand the mechanisms involved, as well as the dependence of damage on composition. Although optical sensitivity is usually the most important detector parameter, increases in dark current and noise can also be significant.

Chapter 3

3 Sample specification and characterisation techniques

3.1 Photoconductors

Most modern photodetectors operate on the basis of the internal photoelectric effects in which the photo-excited carriers (electrons and holes) remain within the sample. Detectors based on photoconductivity rely directly on the light-induced increase in the electrical conductivity of a material. The electrical conductivity of the material σ increases in proportion to the photon flux ϕ. An electric field applied to the material by an external voltage source causes the electrons and holes to be transported. This in turn results in a measurable electric current in the circuit. Photoconductive detectors operate by registering either the photocurrent I_p, which is proportional to the photon flux ϕ, or the voltage drop across a load resistor R placed in series with the circuit.

Photoconductivity is a well-known property of semiconductors in which the electrical conductivity changes (usually increases) due to the incident radiation [44, 45].

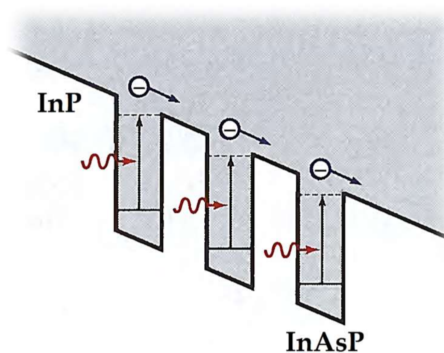

Figure 3.1: Generation of mobile charge carriers by absorption of photons in a QWIP. The device is configured such that there is a single energy level in each well, corresponding to sensitivity in a particular spectral band. The detector illustrated comprises InP barriers and InAsP quantum wells, providing the electrons that occupy the energy levels.

Photoconductivity involves several successive or simultaneous mechanisms, namely absorption of the incident light, carrier photo-generation, and carrier transport (including carrier trapping, de-trapping and recombination). The magnitude of the conductivity change induced by irradiation depends upon the number of carriers produced per absorbed photon, and the mobility of photo-generated carriers and extraction of carriers to external circuit. The duration of this change depends on many factors, such as the lifetime of the carriers and the time for the carriers to encounter a

trap. Therefore, photoconductivity is also a valuable probe for the electronic properties of semiconductors relating to the charge carrier mobility and lifetime. Furthermore, photoconductive materials find a wide variety of applications in photodetectors [46] and photovoltaic devices [47].

Properly configured heterostructures can serve as useful photoconductive detectors. One example is the quantum-well infrared photodetector (QWIP). QWIPs fabricated from III-V compound semiconductors offer high responsivity from mid- to far-infrared wavelengths ($\lambda \sim 4$ - $20\ \mu m$) and high speeds, but require cooling. Multiple heterostructures are designed by surrounding a thin layer of a small bandgap material with a higher bandgap semiconductor. The formed potential wells spatially confine electrons and/or holes. Exploiting sufficiently thin quantum wells (QWs) results in a quantisation of the energy levels and strongly modified density of states. In the darkness at low temperature, the charge carriers (which are typically electrons, but could be holes) are trapped in the QWs. Incident infrared photons release the electrons occupying a bound energy level in the QWs to the continuum, thereby creating a mobile charge carrier that increases the conductivity of the material (see Fig. 3.1). Consequently, these confined energy levels can be utilised to change device parameters, for example, the absorption wavelength range. The energy difference in such cases is typically small, providing a detection capability of MWIR/LWIR [1] photons. However, it is necessary to keep the quantum well populated with carriers for the possibility of an intersubband transition. This is typically obtained by a p-i-p or n-i-n photoconductor geometry. The quantum dots infrared photodetector (QDIP), a variation on this theme, can also be used for multi-wavelength infrared detection via intersubband transitions.

More recently, low-dimensional semiconductor systems e.g. NW arrays have attracted a growing interest for photovoltaics, fast photodetectors and highly integrated optoelectronic devices and interconnects [48], optical interconnects [49]. A notable major advantage of NWs stems from nanophotonic resonances [50] exhibited when the diameter and pitch of NW arrays are optimised for the desired detection wavelength [51]. These effects have been utilised in InP NW-based solar cells achieving 13.8% and 15.3% efficiency [52, 53].

3.2 Nanowire-based photodetectors

In the last decade, one-dimensional or quasi-one-dimensional NWs have been widely researched as potential building blocks for nanoelectronic circuits [54, 55]. Thanks to the ongoing advancement in the growth and fabrication methodologies, by means of either top-down or bottom-up approach, NWs can be now realized out of a variety of functional materials (e.g., semiconductors metals, superconductors). On the pathway to nanoscale integration, this opens up new opportunities toward understanding and

[1] Medium wavelength infrared (MWIR, 3 - 5 μm), Long wavelength infrared (LWIR, 8 - 14 μm)

utilising the unique physical properties of these low-dimensional systems, such as their thermoelectric properties [56], quantum size effects, or enhanced biological and chemical sensitivity [57].

Even above the quantum confinement size-regime, NW photoconductors can yield higher light sensitivity than their bulk counterparts due to the large surface-to-volume ratio and small dimensions [58]. Moreover, the possibility to integrate axial and radial heterostructures in NWs enables large scale integration of novel sensors with better performance and extended functionality. The small footprint of NWs, also makes it possible to integrate the sensors with main-stream silicon technology.

3.2.1 InP NW-based photodetectors

Indium phosphide is an important III–V semiconductor, crystallised in two crystalline structures wurtzite (WZ) and zinc blende (ZB) in nanostructures with direct band gaps of 1.42 eV and 1.35 eV at room temperature, respectively. Therefore, making that suitable for infrared photodetectors and is a highly promising candidate for the construction of viable nano-integrated circuits [59]. Compared to other III-V compound semiconductors, InP has been used in high-power and high-frequency electronics because of high electron mobility and relatively large bandgap. Lieber's group [60] successfully demonstrated the first grown InP NW-based p-n junction by using laser-assisted catalytic growth method. Extensive studies on optimization of growth of homo- and heterostructure NWs have also been done in parallel at Lund University.

3.2.1.1 InP/InAsP NW-based QDiscs-in-wire photodetectors

QWIPs are suitable for large array fabrication as the epitaxial grown material is of excellent quality and uniformity. In order to commercially expand the use of infrared imaging in emerging applications such as industrial process control, novel detector concepts are required to reasonably lower the fabrication and operation costs. The 1D geometry of NWs, combined with quantum confinement structures provides added design features for such detectors. Essential for efficient NW-based QWIPs is a strong confinement of carriers in the quantum wells.

The relatively large conduction band offset in the InP/InAsP system strongly confines carriers leading to higher operating temperatures in lasers and decreases the leakage current in detectors [61]. Implementing this material system in a NW geometry combines the advantages of the small footprint, bandgap tuning and confinement in quantum discs (QDiscs) for ultimate monolithic integration of photonics with main-stream silicon CMOS driver/read-out electronics.

Furthermore, by incorporating InAsP quantum discs (QDiscs) into a n^+-i-n^+ InP NW array photoconductor geometry, we are potentially benefiting from quantum structures in increasing the resistance of our devices in radiation-harsh environments.

3.3 Growth, processing and sample specification

All samples and devices studied in this project are based on large arrays of millions of InP NWs, vertically grown by MOVPE at NanoLund, comprising 20 InAsP QDiscs, on n^+-InP substrates. As indicated in Fig 3.2 a, each individual NW comprises an n^+-i-n^+ geometry with incorporated InAsP QDiscs in the i-segment. To optimize the dark current of the devices, the unintentional n-doping in the nominally intrinsic NW section was compensated by *in-situ* Zn doping [46, 62].

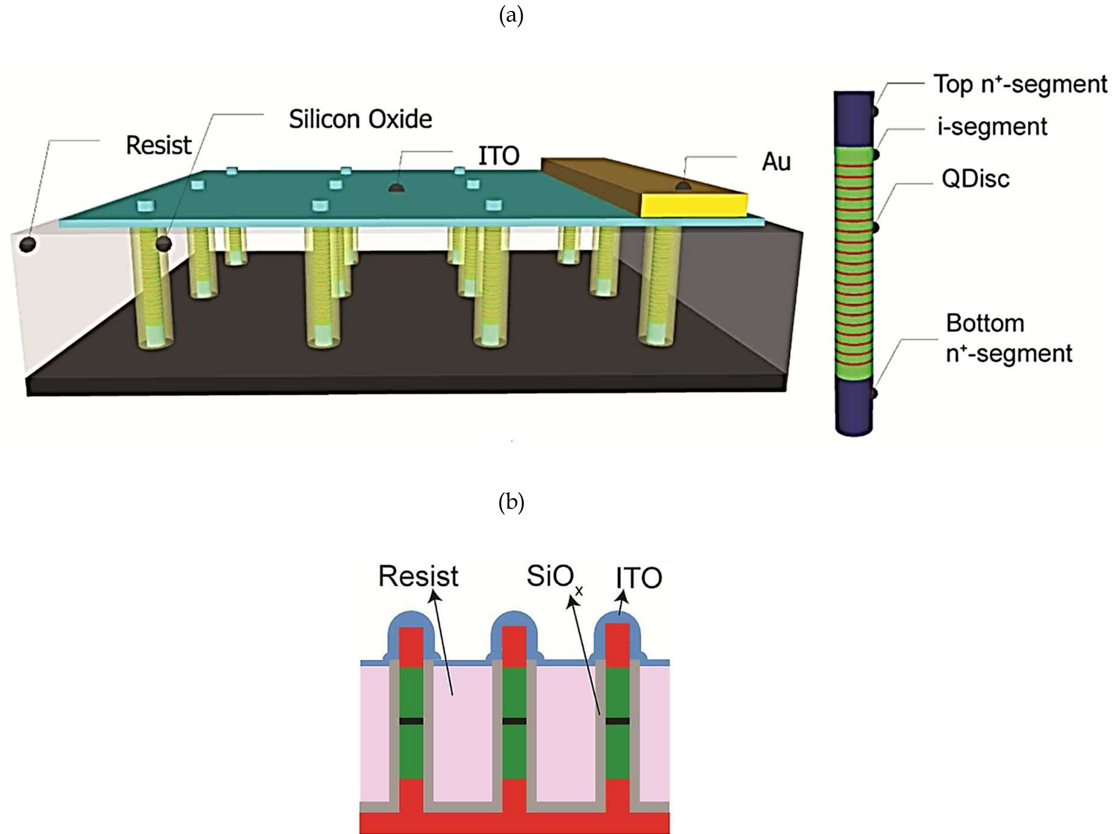

Figure 3.2: (a) Schematics of a vertically processed 20 QDiscs-in-wire array detector. (b) Processing scheme with ITO sputtered on top of the resist acting as spacer layer to prevent side-gating effects [46].

The growth was already carried out, at NanoLund group, in a low-pressure Aixtron 200/4 MOVPE at 440 °C. The InAsP QDiscs were grown by turning off the trimethyl-indium (TMIn) flow and replacing the phosphine (PH3) with arsine (AsH3) for 2 s. For further details, the interested reader can refers to reference [62].

Using atomic layer deposition (ALD), the vertical processing of the NW arrays was conducted based on deposition of 50 nm of SiO_x, followed by 5 nm of Al_2O_3. A photoresist (S1813) was spin-coated and back-etched in reactive ion etching (RIE) to expose 200-250 nm of the NW tips. The SiO_x and Al_2O_3 were removed using buffered oxide etch (BOE), and subsequently, the gold catalyst particles were removed by

chemical solvents [63]. Then, as it can schematically be seen from Fig. 3.2 b, the thick photoresist layer was hard-baked and then after a 50 nm NW side-wall coverage was obtained by sputtering indium tin oxide (ITO) as a transparent top contact. Finally, two layers of 20 nm Ti and 400 nm Au were evaporated as bond pads (Fig. 3.2. a).

The grown NWs had a diameter of 130 nm and a length of 2 μm (Figure 3.3 a) and the centre-to-centre distance (pitch) between two consecutive NWs was 400 nm. The thicknesses of grown QDiscs are 10±1 nm, as observed in TEM (Fig. 3.3 b). Energy dispersive X-ray spectroscopy (EDX) has revealed sharp InAsP/InP interface transitions (Figure 3.3 b). The separation between the QDiscs varied from 50 nm at the base to 25 nm at the tip of the NWs (Figure 3.3 d). This decrease in InP barrier thickness is consistent with the drop in growth rate with the length of pure InP NWs which occurs due to a decreased In supply from the substrate surface.

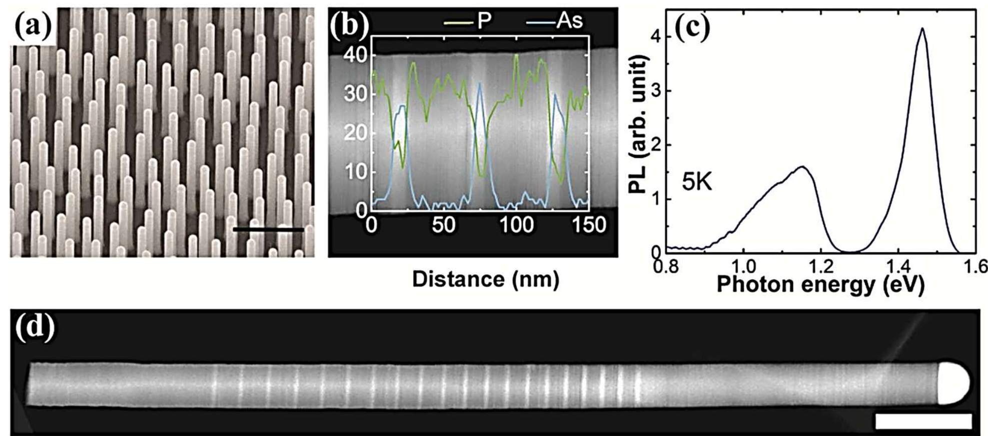

Figure 3.3: (a) SEM image of an as-grown InP n+-i-n+ NW array with 20 InAsP QDiscs in each NW. The scale bar is 1 µm. (b) EDX line scans overlaid on a TEM image of a NW. Green (blue) colour represents P (As), respectively. (c) Typical PL and (d) TEM of a representative NW. The scale bar is 200 nm.

Previously measured photoluminescence (PL) uncovered a relatively broad peak between 0.9 eV and 1.2 eV at 5 K (Figure 3.3 c) which is attributed to QDiscs implanted in i-segment. The peak width most likely reflects the combination of variations in QDisc thicknesses and composition [64, 65].

3.4 Characterization techniques

In this section, the different optoelectronic characterization techniques are described.

3.4.1 Fourier transform infrared spectroscopy

Fourier transform infrared (FTIR) spectroscopy is based on the principle of Michelson interferometer (Fig. 3.4). In a Michelson interferometer a beam from an external light source is divided into two branches by a semi-transparent beam splitter. The two branches propagate towards two mirrors, one fixed and one moving, where the beams

are reflected back towards the beam splitter. The interference between the two beams, when they recombine at the beam splitter, will vary with the optical path difference (OPD) introduced between the two beams. When the OPD is zero or a multiple of the wavelength of the incident beam, the two beams interfere constructively and the amplitude of the resulting beam is twice the amplitude of a single beam. When the OPD is one half of the wavelength of the incident beam, the intensity of the two beams cancel through destructive interference. Consequently, the intensity (I) of the resulting beam leaving the interferometer is modulated with a modulation frequency which depends on the wavelength (λ) of the incident beam and on the introduced OPD (δ). This dependence is given in equation 3-1, where the variation of the OPD with the scanning speed (v) of the mirror ($\delta = 2vt$) has been inserted.

Equation 3-1 $$I(\delta) \propto \cos\left(2\pi\frac{\delta}{\lambda}\right) = \cos\left(4\pi\frac{vt}{\lambda}\right)$$

Simultaneous modulation of a wide wavelength spectrum is enabled in FTIR spectroscopy, since each wavelength gives rise to a unique modulation frequency, $\frac{2v}{\lambda}$.

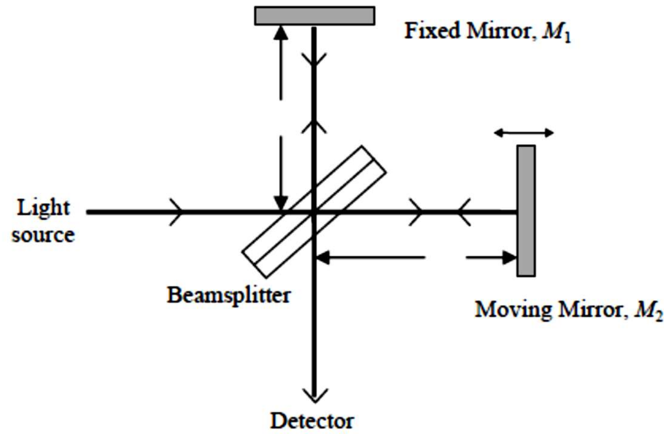

Figure 3.4: Schematic picture of the principle of a Michelson interferometer, which creates modulated beam by introducing an optical path difference (OPD) between the transmitter and the reflected beam.

The resulting intensity of the outgoing beam is then the sum of all wavelength components, given by equation 3-2, which can be recognized as the Fourier transform of the spectral distribution. The spectrum, $I(\lambda)$ can consequently be obtained by inverse transformation of the obtained signal.

Equation 3-2 $$I(\delta) \propto \int_0^\infty I(\lambda)\cos\left(4\pi\frac{vt}{\lambda}\right)d\lambda = \int_0^\infty I(\lambda)e^{4\pi\frac{vt}{\lambda}}\,d\lambda$$

FTIR spectroscopy is a powerful technique capable of measuring spectrally resolved absorption, transmission, PL and photocurrent with a high signal-to-noise (SNR) ratio and short measurement time. Since photocurrent (PC) measurements has been utilised in this work, it will be described in the next sections.

3.4.2 Fourier transform photocurrent measurements

In Fourier transform photocurrent (FTPC) measurements, a broadband source is used to excite carriers and the sample itself is used as a detector (Fig. 3.5). A bias is applied to the sample which forms a closed circuit with a fast current-voltage amplifier. The amplified and converted PC is modulated by the moving mirror as explained above. The PC signal versus mirror position is called the interferogram and it is subsequently Fourier transformed to extract the spectrally resolved PC. FTPC measurements can be used to detect intersubband as well as interband transitions. Photocurrent spectra should be normalized with respect to the photon flux to compensate for any variations in the impinging photon flux.

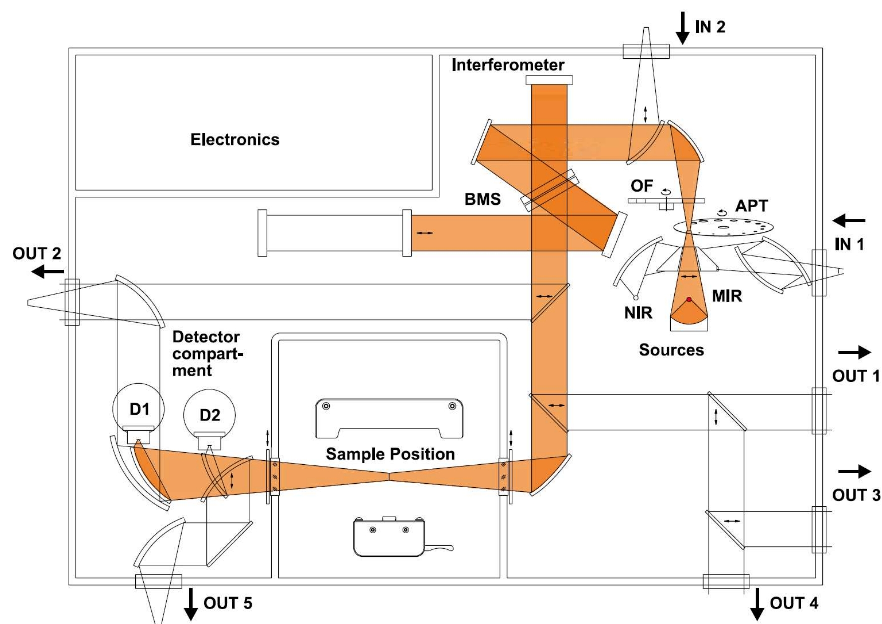

Figure 3.5: Schematic of the experimental setup for Fourier transform photocurrent measurements (FTIR Bruker Vertex 80v setup).

In our measurements, we have used the FTIR model Vertex 80v from Bruker together with an integrated variable-temperature closed-cycle PTSHI-950 cryostat from Janis (inserted into the sample compartment) for temperature-dependent PC measurements in the NIR region (Fig 3.5). A tungsten halogen lamp is used as a broadband light source, along with a CaF_2 beam splitter, while the InP/InAsP NW sample itself is used as a detector. The modulated photocurrent from the sample is amplified using a Keithley 428 programmable current-voltage amplifier. The spectrometer was evacuated to avoid any influence of absorption lines in air.

3.4.3 Dark and photocurrent measurements

Dark current measurements are performed through measurements of the current (I) for different applied voltages (V). Since the dark current is the current present in the structure without excitation from an external source, the sample is totally shielded during the measurements. The shield should be removed under illumination to measure the photocurrent or total current at both room and low temperatures. Variable temperature (5 K – 300 K) I-V measurements were recorded with a Keithley 2636B source meter. The achieved dark current is normalised by the area of the device in order to simplify comparisons with other devices.

Chapter 4

4 Experimental results

All the growth, fabrication and processing of the samples used in this study were done at NanoLund. The irradiation of 1 MeV H^+ ions at room temperature under vacuum conditions were done at the Department of Nuclear physics. To be more specific, further details can be found in Ref. [66, 67]. The ion fluences ranged from 1.0×10^{12} cm^{-2} to 3.0×10^{13} cm^{-2}. The fluence levels were selected on the basis of the recent work on displacement damage in GaAs/AlGaAs core/shell ensemble nanowires [2]. The electrical and optical characterization discussed above was carried out in the Rydberg Laboratory at Halmstad University.

Table 4.1 summarises the different investigated samples S1 and S2 and radiation fluences.

Table 4.1: Overview of samples S1 and S2.

Sample name	Number of included devices	Number of irradiated devices	Radiation fluence p/cm^2
11637 (S1)	6	2	A*: 2.5×10^{13}
11206 (S2)	5	3	A: 3×10^{12} B: 4×10^{12} C: 3×10^{13}

* All the devices are not processed in the same area. Therefore, they are divided into three categories which labeled as A, B, and C. Label A indicates the biggest area and covers a surface of 800×800 μm^2. The other devices labeled as B: 400×400 μm^2, and C: 200×200 μm^2.

According to the Stopping and Range of Ions in Matter (SRIM) Software [68], the ion stopping and range of 1 MeV protons were calculated in InP, assuming a density of 4.81 g/cm^3. The range is about 13 µm, and the energy loss is 51.7 keV/µm for upper 200 nm, then it gradually increases. In principle, the energy loss starts at about 50 keV per micrometre and increases slowly during the first 1.5 µm of NW.

4.1 Pre-radiation FTPC and I-V measurements

In the first step, the PC and I-V characteristics have been recorded for all devices at different temperatures before the ion irradiation.

As it can be seen from Fig. 4.1, the spectrally resolved photocurrent shows a strong increase around 1.4 eV which agrees well with the fundamental energy of bulk InP. This signal comes from the InP NWs. Additionally, there are three different peaks in the photon energy range between 0.5 eV and 1.25 eV that are attributed to interband transitions in the InAsP QDiscs.

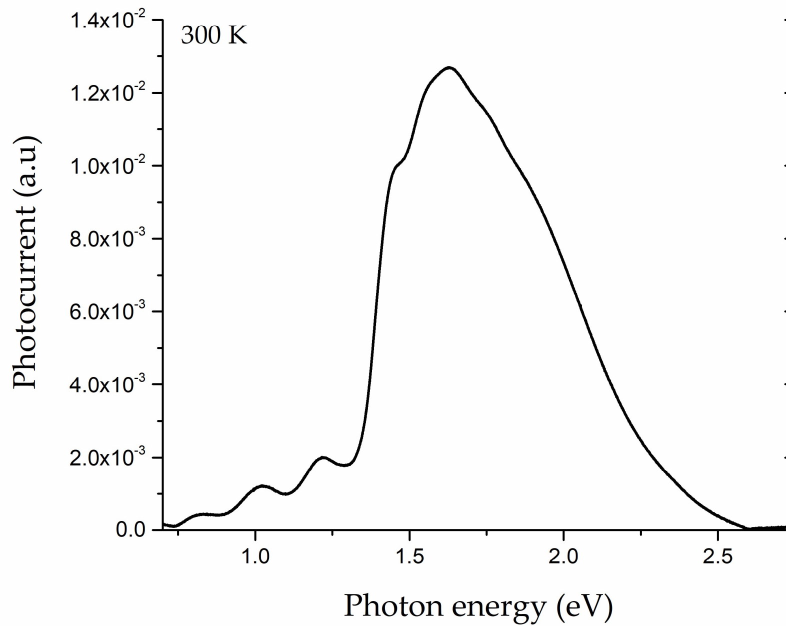

Figure 4.1: Spectrally resolved photocurrent at 1V bias and room temperature.

Figure 4.2) shows the I-V characteristics in dark and under illumination at 300K. A small open-circuit voltage (-0.16 V) is observed under illumination which might reflect a weak overcompensation of the unintentional n-doping in the i-segment by Zn, creating an n^+-p^--n^+ structure instead of an n^+-i-n^+ structure [46].

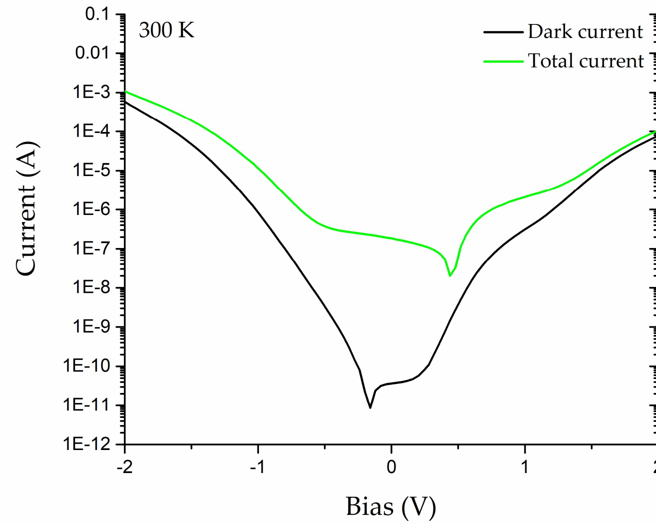

Figure 4.2: I-V characteristic in darkness (black trace) and under illumination (green trace) at 300 K.

The PC (Fig. 4.3) and I-V characteristics (Fig 4.4) were measured at lower temperatures (5 K to 150 K) as well. The PC measurements at lower temperatures still present clear signals in response to photon energies between 0.5 eV and 2.5 eV in comparison with 300 K. A general observation is that the PC is strongly enhanced with increasing the temperature. Furthermore, the relative PC contribution from the QDiscs compared to the InP NW matrix is also enhanced at 150 K compared to 5 K, indicating that the photo-generated carriers are more efficiently extracted from the QDiscs by thermal activation.

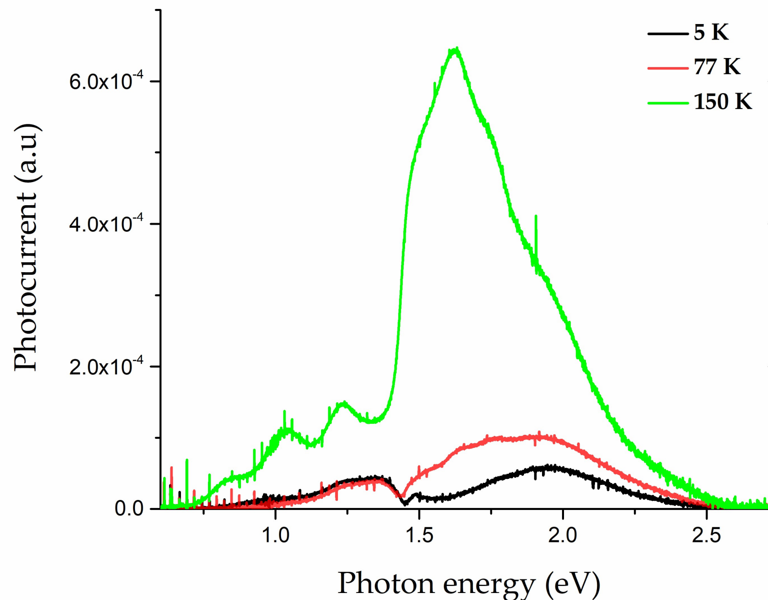

Figure 4.3: Temperature dependence of PC for sample S1 before proton irradiation.

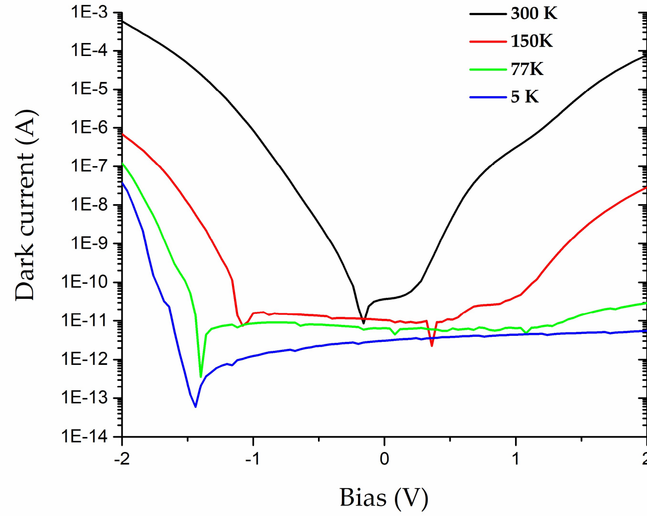

Figure 4.4: Temperature dependence of I-V characteristics in darkness for sample S1 before proton irradiation.

As it can be seen from Fig 4.4, a significant temperature dependence of the dark current was observed with a reduction of about seven orders of magnitude at 2 V bias from 300 K to 5 K. Such a strong temperature dependence illustrates efficient trapping of carriers at low temperatures in the staggered potential landscape introduced by the multiple QDiscs.

4.2 Post-radiation FTPC and I-V measurements

The PC and I-V characteristics were measured in several different time intervals after exposure to investigate possible short- or long-time degradation effects after radiation. For this aim, sample S1 was irradiated with the fluence of 2.5×10^{13} cm^{-2} and characterised in different intervals after radiation. Additionally, to investigate the dependence of radiation fluence on the optoelectronic properties of the exposed devices, sample S2 was irradiated with three various fluences.

4.2.1 Post-radiation PC measurements

Fig 4.5 shows the spectral response of a device in sample S1 in five different elapsed time before and after proton irradiation. Interestingly, the PC measured directly after irradiation significantly increased by about one order of magnitude compared to before the irradiation. In contrast, the PC contributions from the QDiscs totally disappeared after irradiation. Successively, the InP and QDisc PC signals recover with time to pre-irradiation levels. A hypothesis is that the proton irradiation temporarily degrades the QW structures and its relative photocurrent intensity is remarkably

lower than that for InP. Moreover, it is assumed that the effective barrier height probably has been reduced and photo-generated carriers can easily add to photocurrent in the photon energies between 1.5 to 2 eV.

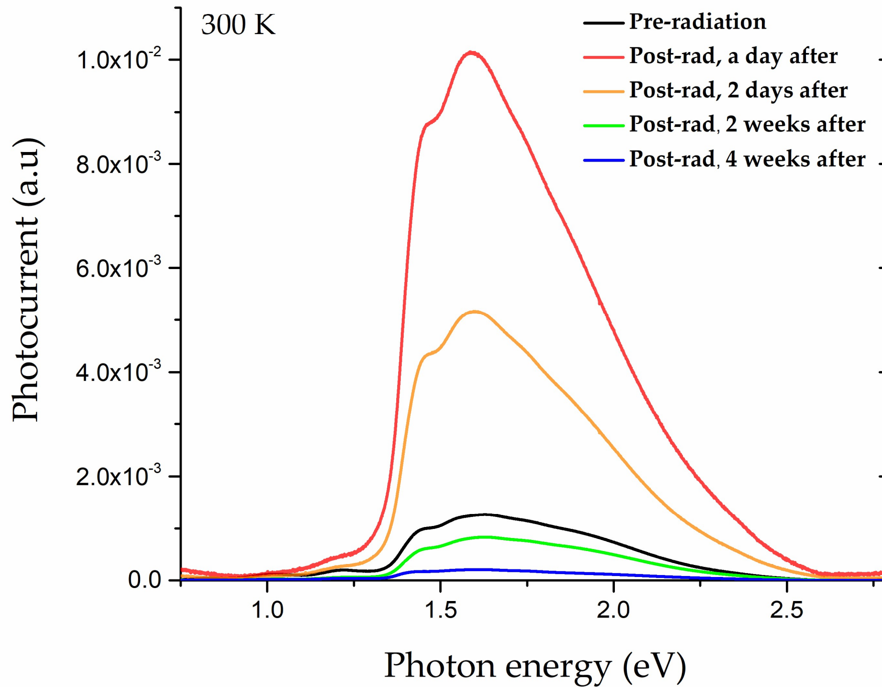

Figure 4.5: Spectral response at 1 V bias at 300 K in five various time intervals irradiated with a fluence of 2.5×10^{13} p/cm^2.

To be more evident and ease comparison, the normalised photocurrent has been presented in Fig. 4.6. Obviously, it shows that the QDisc signals gradually appeared within two weeks after exposure. A speculation is that the relatively modest proton fluence of 2.5×10^{13} p/cm^2 only has a short-time degradation effect on the active regions of the NWs and QDiscs. For better understanding of the radiation effects on QDiscs signals, however, more radiation exposures and characterization techniques, e.g. photoluminescence or time resolved photocurrent, is needed.

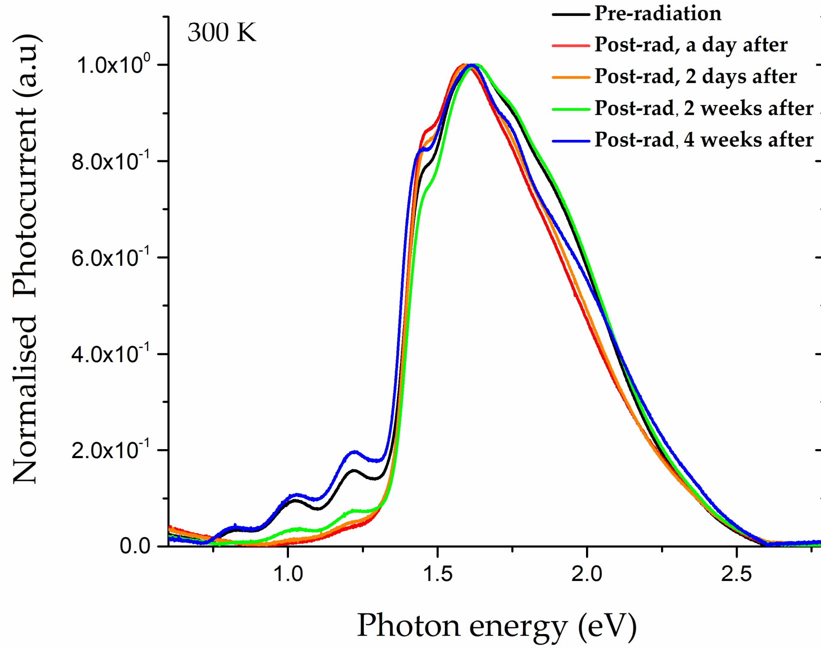

Figure 4.6: Normalised spectral response at 1 bias voltage at 300 K in various time intervals before and after irradiation.

The fact that the PC fully recovers 4 weeks after exposure indicates that InP/InAsP NW photodetectors might be suitable in radiation-harsh environments such as space applications. Considering spectrally resolved photocurrent, the device still indicated even more radiation resistance in lower temperature measurements and other biases (Fig 4.7).

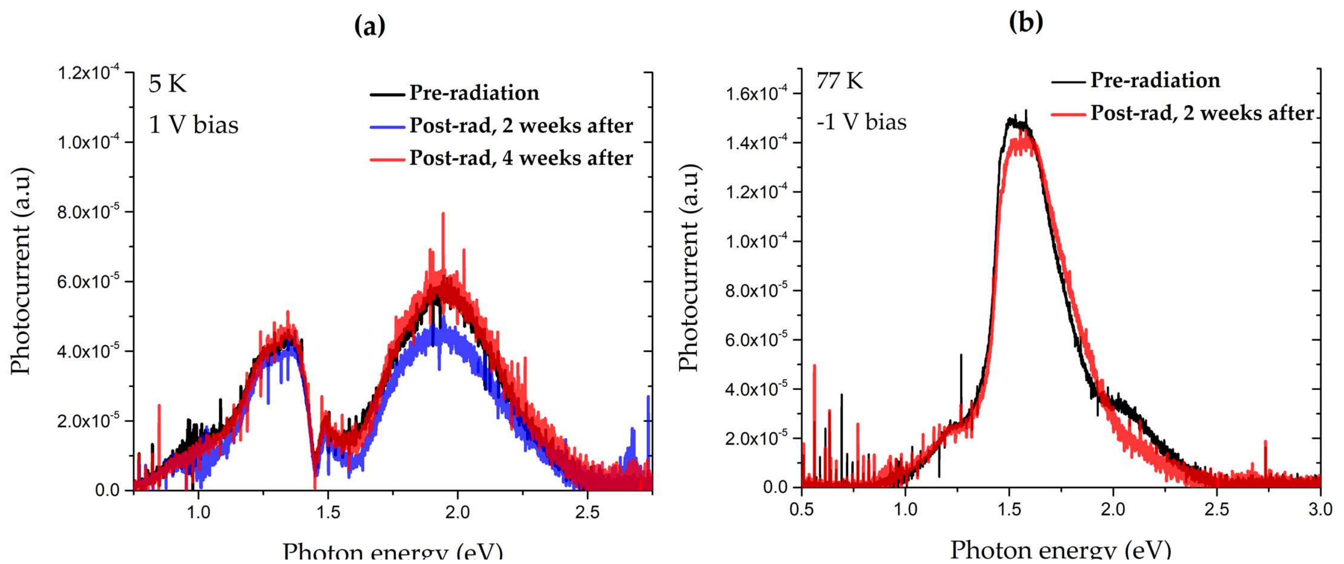

Figure 4.7: PC measurements at (a) 5 K and (b) 77 K after different elapsed time after proton irradiation. Note the different polarity of the applied bias.

4.2.2 Post-radiation I-V characteristics

A noteworthy technic to understand the proton irradiation impacts on InP/InAsP NW arrays is considering changes in the I-V characteristic before and after irradiation. Fig 4.8 shows the interesting behaviour of devices in sample S1 bombarded with the fixed radiation fluence of 2.5×10^{13} p/cm^2. As implied, the dark current dramatically increased after radiation. However, as time goes by, dark current gradually decreased in about 4 weeks after radiation, and pre- (black trace) and post-radiation (blue trace) plots coincided to a large extent.

It is well known that, in general, particle bombardment results in displacement damage in semiconductors which in turn leads to carrier removal and degradation of carrier mobility and lifetime. However, in our case, conductivity was also not stable with time. We interpreted this as the out-diffusion of protons/hydrogen, which were occupying interstitial donor side after irradiation [69].

In addition, the projected energetic protons interact with host semiconductor atoms and produce energetic primary recoils. These recoils displace additional atoms, and those defects give rise to energy levels in the InP bandgap. Levels at or near mid-gap enhance the thermal generation rate in device active regions, and thereby cause the dark current to increase [70].

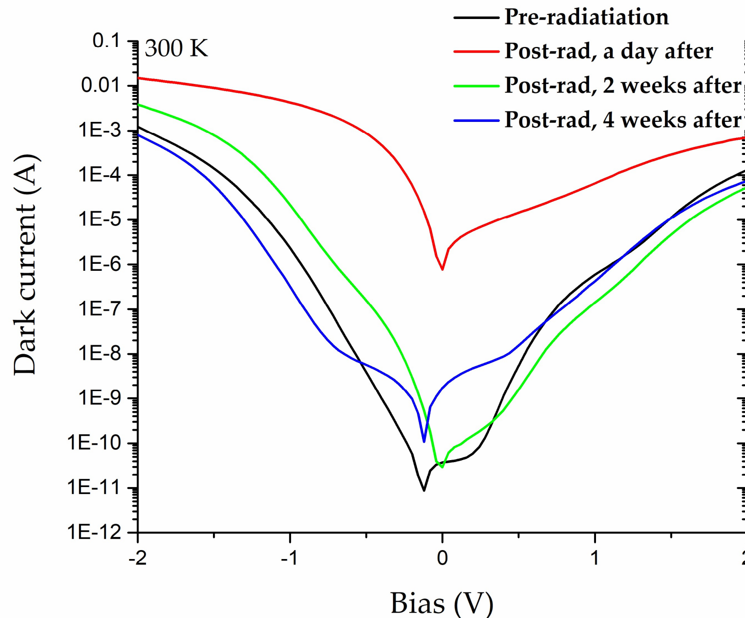

Figure 4.8: Dark current changes before and after proton irradiation with 2.5×10^{13} p/cm^2 at room temperature and different time intervals.

4.3 Fluence-dependence of PC

To estimate the radiation resistance of or NW array detectors, three devices within sample S2 were individually irradiated with three different radiation fluences (Table 4.1), and their optoelectronic performance were studied. Based on the results and PC plot examinations, the spectral response variations of unirradiated/irradiated devices on the reference sample chip S2 were more than 30%, thus making a comparison to be unfair. Therefore, the PC data have been separately plotted and were qualitatively compared.

To begin with, the pre- and post-radiation PC measurements have been presented for the lowest fluence of 3×10^{12} p/cm^2 at room temperature and 0.4 V bias in Fig 4.9. Obviously, the PC rose by a factor of 3 after proton radiation, besides the device responded to all incident photon energies from 0.5 eV to 2.5 eV. That is, the device showed a radiation resistance to low proton fluence. Moreover, the photocurrent signal declined to the level prior to the exposure after 14 days.

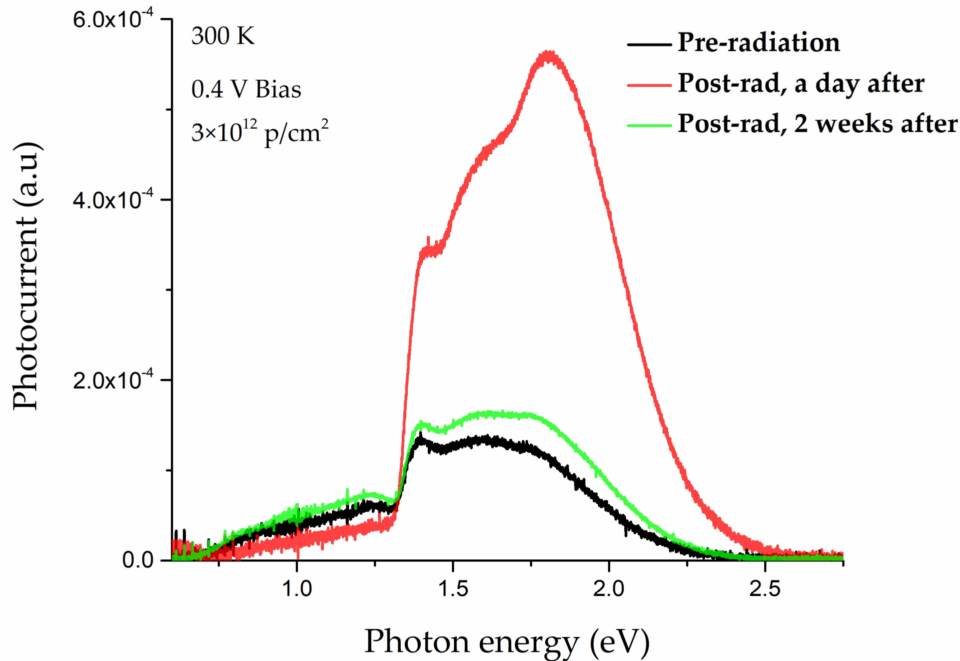

Figure 4.9: Pre- and post-radiation photocurrent vs. photon energy for the lowest proton fluence of 3×10^{12} p/cm^2 at room temperature and 0.4 V bias in different elapsed time.

By increasing the radiation fluence by an order of magnitude, the most significant changes were observed in PC attributed to QDisc structures. Fig 4.10 shows that the related QDisc signals totally disappeared after radiation and the device did not

respond to photon energies between 0.5 eV and about 1.25 eV, however, the device was still alive and sensitive to the incident photon energy corresponding to InP band gap. To make the comparison fair, it should be mentioned that the irradiated device with fluence of 3×10^{13} p/cm^2 had a smaller area (16 times) than that irradiated with 3×10^{12} p/cm^2 fluence in the sample S2. Although InP/InAsP NW array indicated a radiation resist to low and intermediate proton fluence, in higher fluence only quantum well structures were affected by probably a permanent degradation effect.

To make the conclusion fair, more devices should be exposed to higher radiation fluences and further measurement techniques are required.

Finally, measurements on the lower temperature of samples for different proton radiation fluences showed similar trends.

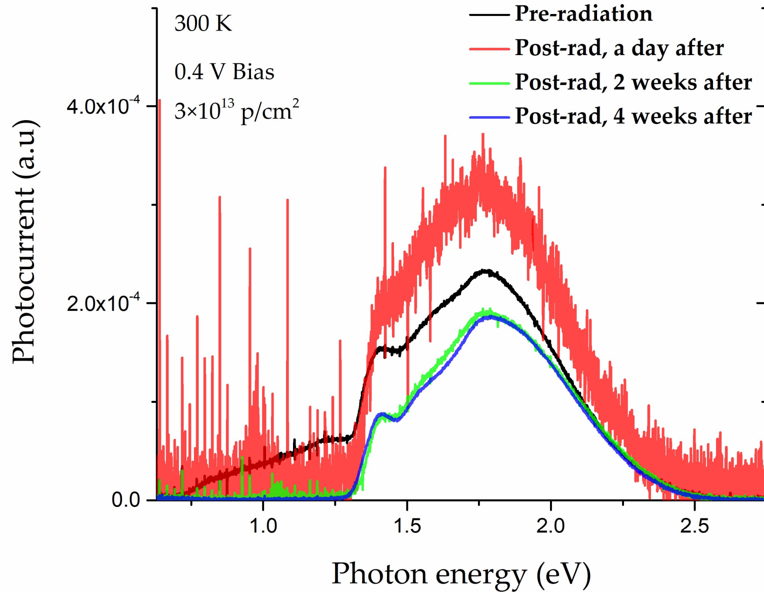

Figure 4.10: Pre- and post-radiation photocurrent vs. photon energy for the highest proton fluence of 3×10^{13} p/cm^2 at room temperature and 0.4 V bias in different time intervals.

4.4 Fluence-dependence of I-V characteristics

Being able to study the proton fluences effects on the NW-based photodetector performance, unlike the spectrally resolved photocurrents, dark currents were normalised to each device area. Fig. 4.11 shows dark current density J vs. voltage V characteristics at 300 K of sample S2 irradiated at different fluence levels.

Analysing the results, it is observed that for the irradiated device at the lowest fluence level, the J-V characteristic increased by an order of magnitude in comparison with the

unirradiated device at 2 V bias. Furthermore, a dramatic enhancement in current density occurred on increase in fluence to 3 x 10^{13} p/cm^2.

A hypothesis is that by bombarding the sample with high energy protons at relatively high fluence levels, displacement damages dominant which in turn can rise the defects rate in the structure. Those defects give rise to deep energy levels in the InP bandgap. Deep Energy Levels at or near mid-gap enhance the thermal generation rate in device active regions and thereby cause the dark current to increase. Each defect acts independently and causes an incremental increase in dark current [71].

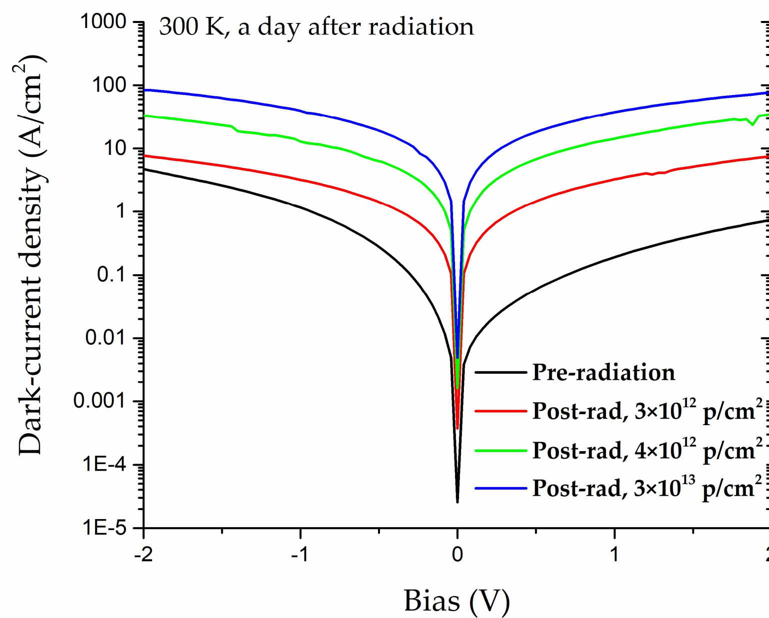

Figure 4.11: Dark current density vs. bias for various proton fluence at room temperature. Measurements conducted a day after irradiation.

In addition, as time goes by, the plots of dark current density progressively decline and approach the pre-radiation conditions (Fig. 4.12). For instance, it is obvious from Fig 4.12 that for the J–V characteristic at the lowest fluence level (3 x 10^{12} p/cm^2, red trace) is very similar to the unirradiated device and roughly undergone a reduction by a factor of eight at bias 2 V. However, for the highest fluence (blue trace) and in a same elapsed time that reduction is a factor of 2.7. As it can be expected, at lower fluences, the device partly offers radiation resistance and it can be concluded that the sample encounters a temporary defect.

It is worth mentioning that the similar trend was also observed at the lower temperatures. To avoid diffuseness, it has been abandoned to present the relevant data.

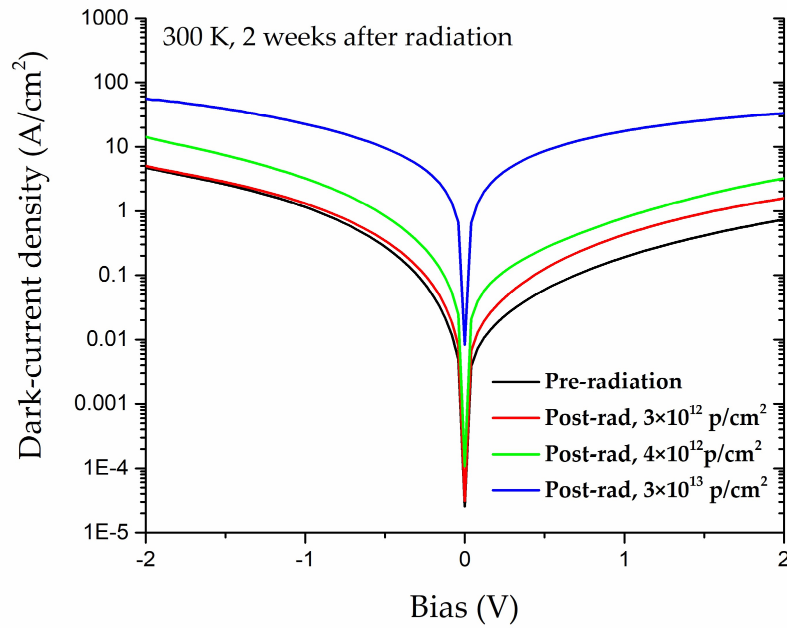

Figure 4.12: Dark current density vs. bias for various proton fluence at room temperature. Measurements repeated 2 weeks after irradiation.

Chapter 5

5 Conclusions

In this work spectrally resolved photocurrents and I-V characteristics have been measured for two samples comprising five devices before and after proton irradiation at various fluences and temperatures. For lower fluence level, it is figured out that photocurrent which attributed to QDiscs disappeared for a couple of days after exposure, however, over time and gradually, those started to manifest again. In contrast, in the highest fluence, no signals were observed for QDiscs after exposure by the end of experimental measurements. This claim can also be proved by observing the I-V characteristics. The initial result can be extracted so far is that the nanowires are somewhat resistant to high-energy radiation at low and intermediate radiation fluences (10^{12}-$4{\times}0^{12}$). Though, we received a short-time degradation effect on our photodetectors that probably related to the ionising effect of high-energy protons.

At the higher radiation fluence, all the devices are still alive and sensitive to Infrared photon energies around 1.4 eV; However, it seems that there is a permanent displacement damage, that is the quantum structures implanted in the i-segment within nanowire completely destroyed by 1MeV proton at the fluence of $3{\times}10^{13}$. Nonetheless, to be more confident, we need to conduct more and deeper investigation for this assert.

Moreover, since our device is a unipolar one, the effect of the radiation-induced defects is to remove electrons from the QDiscs, and the dark current depends strongly on electron density.; the absorption, however, is directly proportional to the electron density. Thus, the dark current is more sensitive to radiation damage than the detector response is. Furthermore, it seems that the effect of defects in the barrier tends to decrease the effective barrier height, which will lead to a further decrease in the current; and, in addition, displacement damage in InP leads to degradation of carrier mobility and lifetime.

Acknowledgments

Gratitude makes sense of our past, brings peace for today, and creates a vision for tomorrow. It gives me immense pleasure to express my sincere gratitude to my main supervisor Prof. Håkan Pettersson at Halmstad University. I thank him for giving me the opportunity to work here and for always being available for guidance, support, discussions, in FTIR laboratory and as an office-mate. His precise guidance and discussions have been always my main lead in this work and undoubtedly in my upcoming research.

I would also like to extend my sincere thanks to my supervisor Prof. Jan Pallon at Nuclear Physics Department, Lund University, for his extremely worthwhile and helpful guidance, also for sharing his valuable experiences and knowledge in the field of Ion Beam Analysis Facility and high-energy radiations during the course of my work in the last few months.

Technology has made it easier for students to learn with new devices, but nothing can come close to the experience of being taught by an inspirational teacher.

Special thanks to my friend Mohammad Karimi, a PhD student at NanoLund group, which provided me InP/InAsP NW array samples and his fruitful help with operating FTIR spectrometer and conveying his knowledge regarding sample specification, characterization etc.

I would like to thank Dr Linus Rose at Ion Beam Accelerator, for introducing me to the proton irradiation and preparing the equipment for sample bombardment.

Now, it is time to express my sincere feelings towards my wife Arezo who has been the source of love and patience that I used to lean against whenever the tasks stick and the work hits harder.

Finally, I will be forever indebted to my parents and family for believing in me and for showering their love even though we are so far apart.

Bibliography

[1] T. Shen, “Radiation tolerance in a nanostructure: Is smaller better?,” *Nuclear Instruments and Methods in Physics Research B* , vol. 266, p. 921–925, 2008.

[2] F. Li, Z. Li, L. Tan and Y. Zhou, “Radiation effects on GaAs/AlGaAs core/shell ensemble nanowires and nanowire infrared,” *Nanotechnology,* vol. 28, no. 12, 2017.

[3] S. Glasstone and P. J. Dolan, The Effects of Nuclear Weapons, Warren: MI: Knowledge Publications, 2006.

[4] A. Belousov, Radiation Effects on Semiconductor Devices in High Energy Heavy Ion Accelerators, Darmstadt, Technical University: Ph.D. Thesis, 2014.

[5] J. F. Ziegler, H. W. Curtis, H. P. Muhlfeld and B. Chin, “IBM experiments in soft fails in computer electronics (1978–1994),” *IBM Journal of Research and Development - Special issue: terrestrial cosmic rays and soft errors,* vol. 40, no. 1, pp. 3-18, 1996.

[6] D. Saxsena, S. Mokkapati , P. Parkinson, N. Jiang, Q. Gao, H. H. Tan and C. Jagadish, “Optically pumped room-temperature GaAs nanowire lasers,” *Nature Photonics,* vol. 7, no. 12, p. 963–968, 2013.

[7] J. Vishal, A. Nowzari, J. Wallentin, M. T. Borgström and et al., “Study of photocurrent generation in InP nanowire-based p+–i–n+ photodetectors,” *Nano Research,* vol. 7, no. 4, p. 544–552, 2014.

[8] E. M. Gallo, G. Chen, M. Currie and T. McGuckin, “Picosecond response times in GaAs/AlGaAs core/shell nanowire-based photodetectors,” *Applied Physics Letters,* vol. 98, no. 24, p. 241113, 2011.

[9] H. Goto, K. Nosaki, K. Tomioka, S. Hara, K. Hiruma and J. Motohisa, “Growth of Core-Shell InP Nanowires for Photovoltaic Application by Selective-Area Metal Organic Vapor Phase Epitaxy,” *Applied Physics Express,* vol. 2, no. 3, p. 5004, 2009.

[10] S. Yu, J. Kupecy and B. Witzigmann, “Electro-Optical Modeling of InP Nanowire Solar Cells: Core-shell vs. Axial Structure,” in *Numerical Simulation of Optoelectronic Devices*, Atlanta, GA, USA, 2010.

[11] H. Melchiro, M. B. Fisher and F. R. Arams, “Photodetectors for optical communication systems,” *Proceedings of the IEEE,* vol. 58, no. 10, pp. 1466 - 1486, 1970.

[12] J. W. Beletic, R. Blank, D. Gulbransen, D. Lee and et al., “Teledyne Imaging Sensors: infrared imaging technologies for astronomy and civil space,” *High Energy, Optical, and Infrared Detectors for Astronomy III,* vol. 7021, 2008.

[13] Z. L. Liu Ru-Shi., “Solar Cell as an Energy Harvesting Device,” *Electrochemical Technologies for Energy Storage and Conversion,* vol. 1&2, 2012.

[14] A. M. Joshi, F. Heine and T. Feifel, “Rad-hard ultrafast InGaAs photodiodes for space applications,” *Spaceborne Sensors III,* vol. 6220, p. 22003, 2006.

[15] C. Poivey, “Radiation Hardness Assurance for Space Systems,” *NASA, GSFC, USA,* 2002.

[16] M. Demkowicz , P. Bellon and B. Wirth, “Atomic-scale design of radiation-tolerant nanocomposites,” *MRS Bull.,* vol. 35, p. 992–8, 2010.

[17] C. H. Li, H. L. Lu, Y. M. Zhang, M. Liu and X. H. Zhao, “Proton-Induced Degradation of InP/InGaAs HBTs Predicted by Nonionizing Energy Loss Model,” *IEEE TRANSACTIONS ON NUCLEAR SCIENCE,* vol. 62, no. 3, pp. 1336-40, 2015.

[18] A. Shatalov, S. Subramanian, S. Chandrasekhar, A. Dentai and et al., “Electron irradiation effects in polyimide passivated InP/InGaAs single heterojunction bipolar transistors,” *IEEE Transactions on Nuclear Science,* vol. 46, no. 6, pp. 1708-1715, 1999.

[19] A. Shatalov, S. Subramanian and A. Dentai, “Neutron irradiation effects in InP/InGaAs single heterojunction bipolar transistors,” *IEEE Transactions on Nuclear Science,* vol. 47, no. 6, pp. 2551-2556, 2000.

[20] C. F. Lo, H. Y. Kim and J. Kim, “Proton irradiation effects on Sb-based heterojunction bipolar transistors,” *Journal of Vacuum Science & Technology B,* vol. 27, no. 6, 2009.

[21] M. Yzmzguchi, C. Uemura and A. Yamamoto, “Electron Irradiation Damage in Radiation-Resistant InP Solar Cells,” *Japanese Journal of Applied Physics,* vol. 23, no. 3, pp. 302-307, 1984.

[22] M. Yamaguchi and K. Ando, “Mechanism for radiation resistance of InP solar cells,” *Journal of Applied Physics,* vol. 63, pp. 5555-62, 1988.

[23] P. L. Gareso, H. H. Tan, J. Wong-Leung and C. Jagadis, “Proton Irradiation Induced Intermixing in InGaAs/InP Quantum Wells,” *Semiconductor Science and Technology,* vol. 21, no. 1441, pp. 93-96, 2006.

[24] M. Boutillier, O. Gauthier-Lafaye , S. Bonnefont , F. Lelarge, B. Dagens, D. Make and O. L. Gouezi, “Proton irradiation effects on InAs / InP quantum dash laser diodes emitting at 1.55 µm,” in *IEEE*, Deauville, France, 2009.

[25] S. B. Witmer, S. D. Mittleman and S. J. Pearton, “Radiation effects on InP-based heterojunction bipolar transistors,” in *InP HBTs: Growth, Processing, and Applications, 1st ed. B. Jalali, S.J. Pearton*, Eds. Boston, Artech House Publishers, 1995, pp. 195-228.

[26] A. Bandyopadhyay, S. Subramanian and S. Chandrasekhar, “Degradation of dc characteristics of InGaAs/InP single heterojunction bipolar transistors under electron irradiation,” *IEEE, Trans. Nucl. Sci,* vol. 46, pp. 840-849, 1999.

[27] A. Shatalov, S. Subramanian, S. Chandrasekhar, A. Dentai and S. M. Goodnick, “Electron irradiation effects in polyimide passivated InP/InGaAs single

heterojunction bipolar transistors," *IEEE Trans. Nucl Sci.,* vol. 46, pp. 1708-1714, 1999.

[28] S. Wolf and R. N. Tauber , Silicon processing for the VLSI era, California: Lattice press, 2000.

[29] A. Holmes-Siedle and L. Adams , Handbook of radiation effects, Oxford: Oxford University Press, 1993.

[30] J. L. Barth, Modeling space radiation environments, Proc 1997 NSREC ShortCourse: Snowmass, 1997.

[31] E. G. Stassinopoulos, G. J. Brucker, D. W. Nakamura, C. A. Stauffer, G. B. Gee and J. L. Barth, "Solar flare proton evaluation at geostationary orbits for engineering applications," *IEEE Trans Nucl Sci,* vol. 43, no. 2, pp. 369-382, 1996.

[32] C. Bussolati and . A. Fiorentini, "Energy for Electron-Hole Pair Generation in Silicon by Electrins and Protons," *Phys. Rev.,* vol. 136, no. 6A, pp. A1756-A1758, 1964.

[33] P. W. Marshall and C. J. Dale, "Space Radiation Effects on Optoelectronic materials for a 1300 nm Fiber Optic Data Bus," *IEEE Trans. Nucl. Sci,* vol. 39, no. 6, p. 1989, 1992.

[34] C. Dale and P. Marshall , "Displacement damage in Si imagers for space applications," *Proc SPIE Charged-Coupled Devices and Solid State Optical Sensors II,* vol. 1447, pp. 70-86, 1991.

[35] V. A. J. Van Lint , R. E. Leadon and J. F. Colwell , "Energy Dependence of Displacement Effects in Semiconductors," *IEEE Trans. Nucl. Sci.,* vol. 19, no. 6, pp. 181-185, 1972.

[36] O. L. Curtis, J. W. Cleland, . J. H. Crawford Jr., J. C. Pigg and et al., "Effect of Irradiation on the Hole Lifetime of n-Type Germanium," *J. Appl. Phys,* vol. 28, p. 1161–1165, 1957.

[37] S. R. Messenger, R. J. Walters, M. A. Xapsos, G. P. Summers and E. A. Burke, "Carrier Removal in p-Type InP," *IEEE Trans. Nucl. Sci.,* vol. 45, no. 6, p. 2857–2860, 1998.

[38] C. Claeys and E. Simoen, Radiation Effects in Advanced Semiconductor Materials and Devices, Berlin: Springer, 2002.

[39] J. M. McGarrity, et al., F. McLean, W. DeLancey, J. Palmour, C. Carter, J. Edmond and R. Oakley, "Silicon Carbide JFET Radiation Response," *IEEE Trans. Nucl. Sci.,* vol. 39, no. 6, p. 1974–198, 1992.

[40] A. H. Johnston, "Radiation Effects in Light-Emitting and Laser Diodes," *IEEE Trans. Nucl. Sci.,* vol. 50, no. 3, p. 689–703, 2003.

[41] O. Gillard, "Theoretical Study of Radiation Effects on GaAs/AlGaAs and InGaAsP/InP Quantum-Well Laser," *J. Appl. Phys., ,* vol. 93, no. 4, p. 1884–1888, 2003.

[42] A. . L. Barry, A. Houdayer, P. Hinrichsen, W. Letourneau , J. Vincent and et al., "The Energy Dependence of Lifetime Damage Constants in GaAs LEDs for 1–500 MeV Protons," *IEEE Trans. Nucl. Sci.,* vol. 42, no. 6, p. 2104–2107, 1995.

[43] P. W. Marshall and C. J. Dale, "Space Radiation Effects on Optoelectronic Materials for a 1300 nm Fiber Optic Data Bus," *IEEE Trans. Nucl. Sci.,* vol. 36, no. 6, pp. 1982-1989, 1992.

[44] H. Bube, Photoconductivity of Solids, New York: Wiley, 1960.

[45] R. H. Bube, Photoelectronic Properties of Semiconductors, Cambridge, New York: Cambridge University Press, 1992.

[46] M. A. Karimi, V. Jain, M. Heurlin, A. Nowzari, L. Hussain, D. Lindgren and et al., "Room-temperature InP/InAsP Quantum Discs-in-Nanowire Infrared Photodetectors," *Nano Lett.,* vol. 17, no. 6, p. 3356–3362, 2017.

[47] A. Nowzari, M. Heurlin, J. Jain, K. Storm, A. Hosseinnia, N. Anttu, M. T. Borgström and et al., "A Comparative Study of Absorption in Vertically and Laterally Oriented InP Core–Shell Nanowire Photovoltaic Devices," *Nano Lett.,* vol. 15, no. 3, p. 1809–1814, 2015.

[48] X. Duan, Y. Huang, Y. Cui, J. Wang and C. M. Liebe, "Indium phosphide nanowires as building blocks for nanoscale electronic and optoelectronic devices," *Nature,* vol. 409, p. 66–69, 2001.

[49] M. D. Brubaker, P. T. Blanchard, J. B. Schlager, A. W. Sanders, A. Roshko and et al., "On-Chip Optical Interconnects Made with Gallium Nitride Nanowires," *Nano Lett.,* vol. 13, no. 2, p. 374–377, 2013.

[50] N. Anttu, "Geometrical optics, electrostatics, and nanophotonic resonances in absorbing nanowire arrays," *Optics Letters,* vol. 38, pp. 730-732, 2013.

[51] J. Svensson, N. Anttu, N. Vainorius, B. M. Borg and L.-E. Wernersson, "Diameter-Dependent Photocurrent in InAsSb Nanowire Infrared Photodetectors," *Nano Lett.,* vol. 13, pp. 1380-1385, 2013.

[52] J. Wallentin, N. Anttu, D. Asoli, M. Huffman, I. Åberg, M. H. Magnusson and et al., "InP Nanowire Array Solar Cells Achieving 13.8% Efficiency by Exceeding the Ray," *Optics Limit. Science,* vol. 339, pp. 1057-1060, 2013.

[53] I. Åberg, G. Vescovi, D. Asoli, U. Naseem, J. P. Gilboy and et al., "A GaAs Nanowire Array Solar Cell With 15.3% Efficiency at 1 Sun," *IEEE J. Photovol.,* vol. 6, pp. 185-190, 2016.

[54] Y. Li, F. Qian, J. Xiang and C. M. Lieber, "Nanowire electronic and optoelectronic devices," *Materials Today,* vol. 9, no. 10, pp. 18-27, 2006.

[55] R. Yan, D. Gargas and P. Yang, "Nanowire photonics," *Nature Photonics,* vol. 3, p. 569–576, 2009.

[56] T. T. Vo, A. J. Williamson and V. Lordi, "Atomistic Design of Thermoelectric Properties of Silicon Nanowires," *Nano Lett.,* vol. 8, no. 4, p. 1111–1114, 2008.

[57] Y. Cui, Q. Wei and H. Park, “Nanowire Nanosensors for Highly Sensitive and Selective Detection of Biological and Chemical Species,” *Science,* vol. 293, no. 5533, pp. 1289-1292, 2001.

[58] X. Dai, S. Zhang, Z. Wang, G. Adamo, H. Liu and et al., “GaAs/AlGaAs Nanowire Photodetector,” *Nano Lett.,* vol. 14, no. 5, p. 2688–2693, 2014.

[59] H. A. Fonseka, P. Caroff, J. Wong-Leung, A. S. Ameruddin, H. H. Tan and C. Jagadish, “Nanowires Grown on InP (100): Growth Directions, Facets, Crystal Structures, and Relative Yield Control,” *ACS Nano,* vol. 8, no. 7, p. 6945–6954, 2014.

[60] C. M. Lieber, “Lieber research group,” [Online]. Available: http://cml.harvard.edu/.

[61] Dixit, V.; Singh, Sh. D.; Porwal, S.; Kumar, R.; Ganguli, T.; Srivastava, A. K., “Determination of band offsets in strained InAsP/InP quantum well by capacitance voltage profile and photoluminescence spectroscopy,” *Journal of Applied Physics,* vol. 109, no. 8, p. 083702, 2011.

[62] V. Jain, “III-V Nanowire-based Infrared Photodetectors, Design, Fabrication and Characterization,” in *Doctoral Thesis*, Lund, Printed in Sweden by Media-Tryck, Lund University, 2016, pp. 17-41.

[63] A. Berg, S. Yazdi, A. Nowzari, K. Storm, J. Vish, N. Vainorius, L. Samuelson, J. B. Wagner and M. T. Borgström, “Radial Nanowire Light-Emitting Diodes in the (AlxGa1−x)yIn1−yP Material System,” *Nano Lett.*, vol. 16, no. 1, pp. 656-662, 2015.

[64] L. Yan, S. Jahangir, S. A. Wight, B. Nikoobakh and J. M. Millunchick, “Structural and Optical Properties of Disc-in-Wire InGaN/GaN LEDs,” *Nano letters,* vol. 15, no. 3, pp. 1535-1539, 2015.

[65] P. Kuyanov and R. LaPierre, “Photoluminescence and photocurrent from InP nanowires with InAsP quantum dots grown on Si by molecular beam epitaxy,” *Nanotechnology,* vol. 26, no. 31, p. 315202, 2015.

[66] P. Kristiansson, M. Borysiuk, N. Arteaga-Marrero, M. Elfman, E. J. Nilsson, C. Nilsson and J. Pallon, “A pre-sample charge measurement system for quantitative NMP-analysis,” *Nuclear Instruments and Methods in Physics Research B,* vol. 268, p. 1727–1730, 2010.

[67] K. G. Malmqvist, G. Hyltén, M. Hult, K. Håkansson, J. M. Knox, N. P.-O. Larsson, J. Pallon and et al., “Dedicated accelerator and microprobe line,” *Nuclear Instruments and Methods in Physics Reaserch,* vol. B77, pp. 3-7, 1993.

[68] J. F. Ziegler , “SRIM - The Stopping and Range of Ions in Matter,” [Online]. Available: http://srim.org/.

[69] C. Ronning, C. Borschel, S. Geburt, R. Niepelt, S. Muller, D. Stichtenoth and et al., “Tailoring the properties of semiconductor nanowires using ion beams,” *Phys. Status Solidi B ,* vol. 247, no. 10, p. 2329–2337, 2010.

[70] J. R. Srour and R. A. Hartmann, "Displacement damage effectiveness in irradiated silicon devices," *IEEE Transactions on Nuclear Science, enhanced,* vol. 36, no. 6, pp. 1825-1830, 1989.

[71] J. R. Srour and R. A. Hartmann, "Enhanced displacement damage effectiveness in irradiated Silicon devices," *IEEE Transactions On Nuclear Science,* vol. 36, no. 6, p. 1825, 1989.

Ebrahim Mansouri.
Born in 1984, Shiraz, Iran.
B.Sc. in Physics and M.Sc. in condensed matter Physics.
M.Sc. degree in Electronic Design with a speciality in Nanoelectronics.

PO Box 823, SE-301 18 Halmstad
Phone: +35 46 16 71 00
E-mail: registrator@hh.se
www.hh.se